

การศึกษาสมบัติการยืดหยุ่นของสารเทอร์โรวัลไกท์บางชนิดภายใต้ภาวะ
แรงดันโดยวิธีเฟรสต์พรีนซิเพิล



นายณราศศักดิ์ พันเดช

วิทยานิพนธ์นี้เป็นส่วนหนึ่งของการศึกษาตามหลักสูตรปริญญาวิทยาศาสตรมหาบัณฑิต
สาขาวิชาฟิสิกส์
มหาวิทยาลัยเทคโนโลยีสุรนารี
ปีการศึกษา 2556

**FIRST-PRINCIPLES STUDY OF PRESSURE
DEPENDENT ELASTIC PROPERTIES IN SELECTED
PEROVSKITE MATERIALS**



Narasak Pandech

**A Thesis Submitted in Partial Fulfillment of the Requirements for the
Degree of Master of Science in Physics
Suranaree University of Technology
Academic Year 2013**

**FIRST-PRINCIPLES STUDY OF PRESSURE DEPENDENT
ELASTIC PROPERTIES IN SELECTED PEROVSKITE
MATERIALS**

Suranaree University of Technology has approved this thesis submitted in partial fulfillment of the requirements for a Master's Degree.

Thesis Examining Committee

(Prof. Dr. Santi Maensiri)

Chairperson

(Prof. Dr. Sukit Limpijumnong)

Member

(Assoc. Prof. Dr. Udomsilp Pinsook)

Member

(Dr. Kanoknan Sarasamak)

Member

(Assoc. Prof. Dr. Anan Tongraar)

Member

(Asst. Prof. Dr. Rattikorn Yimnirun)

Member

(Prof. Dr. Sukit Limpijumnong)

Vice Rector for Academic Affairs

And Innovation

(Assoc. Prof. Dr. Prapun Manyum)

Dean of Institute of Science

ณราศีกดิ์ พันเดช : การศึกษาสมบัติการยืดหยุ่นของสารเพอร์โรวสไกต์บางชนิดภายใต้
ภาวะแรงดันโดยวิธีเฟิร์สท์พริન્ซิเพิล (FIRST-PRINCIPLES STUDY OF PRESSURE
DEPENDENT ELASTIC PROPERTIES IN SELECTED PEROVSKITE MATERIALS)
อาจารย์ที่ปรึกษา : ศาสตราจารย์ ดร.ชูกิจ ลิมปิจำนงค์, 108 หน้า.

ในวิทยานิพนธ์ฉบับนี้ได้มีการศึกษาคุณสมบัติความยืดหยุ่นของสารประกอบออกไซด์
แบบเพอร์โรวสไกต์บางชนิด ได้แก่ BeTiO_3 , MgTiO_3 , CaTiO_3 , SrTiO_3 , BaTiO_3 , PbTiO_3 , PbZrO_3
และ PbHfO_3 โดยวิธีคำนวณแบบเฟิร์สท์พริન્ซิเพิล (หรือ แอบ อินิธิโอ) โดยพบว่าค่าคงที่ความ
ยืดหยุ่นที่คำนวณได้นั้นสอดคล้องพอควรกับผลจากการคำนวณและการทดลองที่มีในอดีต สำหรับ
 PbTiO_3 และ PbZrO_3 นั้นได้ศึกษาผลของความดันต่อคุณสมบัติความยืดหยุ่นและความเร็วเสียง
ภายใต้ภาวะความดันในช่วง 0 ถึง 40 จิกะปาสกาล พบว่าค่าคงที่ความยืดหยุ่นและความเร็วเสียงมีค่า
เพิ่มขึ้นตามความดันเกือบจะเป็นรูปแบบการแปรผันตรงในช่วงดังกล่าว โดยค่าคงที่ความยืดหยุ่น
 C_{11} ได้เพิ่มขึ้นอย่างรวดเร็วในขณะที่ค่าคงที่ความยืดหยุ่น C_{12} และ C_{44} มีการเปลี่ยนแปลงกับความ
ดันค่อนข้างน้อย นอกจากนี้แล้วยังได้ศึกษาผลของไอออนบวกที่มีต่อค่าคงที่ความยืดหยุ่น โดย
พบว่าค่าคงที่ความยืดหยุ่น C_{11} จะมีค่าสูงสุดเมื่อขนาดของไอออนบวกที่ตำแหน่ง A และ B มีขนาด
ใกล้เคียงกัน ค่าคงที่ความยืดหยุ่น C_{12} นั้นได้รับอิทธิพลจากไอออนบวกที่ตำแหน่ง B และค่าคงที่
ความยืดหยุ่น C_{44} ได้รับอิทธิพลจากไอออนบวกที่ตำแหน่ง A รายละเอียดและเหตุผลของการ
เปลี่ยนแปลงค่าความยืดหยุ่นกับไอออนบวกแต่ละชนิดได้ถูกอภิปรายในวิทยานิพนธ์นี้

สาขาวิชาฟิสิกส์
ปีการศึกษา 2556

ลายมือชื่อนักศึกษา _____
ลายมือชื่ออาจารย์ที่ปรึกษา _____

NARASAK PANDECH : FIRST-PRINCIPLES STUDY OF PRESSURE
DEPENDENT ELASTIC PROPERTIES IN SELECTED PEROVSKITE
MATERIALS. THESIS ADVISOR : PROF. SUKIT LIMPIJUMNONG,
Ph.D. 108 PP.

ELASTIC PROPERTIES/PEROVSKITE/FIRST PRINCIPLES

In this thesis, the elastic properties of selected perovskite oxides materials, i.e., BeTiO₃, MgTiO₃, CaTiO₃, SrTiO₃, BaTiO₃, PbTiO₃, PbZrO₃ and PbHfO₃, were studied using first principles (or *ab initio*) methods. Our calculated elastic properties are in reasonable agreement with the available theoretical and experimental results. For PbTiO₃ and PbZrO₃, the pressure dependencies of their elastic properties and sound velocities were studied in the pressure range of 0 – 40 GPa. All elastic constants and sound velocities increase with the pressure in this range with an almost perfect linear trend. C_{11} elastic constant rapidly increases with the pressure while C_{12} and C_{44} are found to be less sensitive to the pressure. The effects of cation species on the elastic properties were also investigated. The maximum C_{11} elastic constant is found when the atomic size of the cations at the A-site and B-site are comparable. C_{12} elastic constant is sensitive to B-site cations while C_{44} elastic constant is sensitive to A-site cations. Details and reasons for such dependencies were discussed.

School of Physics

Academic Year 2013

Student's Signature _____

Advisor's Signature _____

ACKNOWLEDGEMENTS

I would like to express the gratitude to my advisors Prof. Dr. Sukit Limpijumnong and Dr. Kanoknan Sarasamak for, their guidance, patience, kind support, and help with the thesis. I thank Prof. Dr. Santi Maensiri, Assoc. Prof. Dr. Udomsilp Pinsook, Assoc. Prof. Dr. Anan Tongraar and Dr. Saroj Rujirawat for contributing as thesis examines committees. I thank Asst. Prof. Dr. Jiraroj T-Thienprasert and Asst. Prof. Dr. Sirichok Jungthawan for their help with some parts of my thesis. I would like to thank the Development and Promotion of Science and Technology Talents Project (DPST, THAILAND) for the scholarship during my master degree program. I acknowledge Synchrotron Light Research Institute for the computation resources. I thank the faculties and friends at the School of Physics, Suranaree University of Technology for their guidances and friendships. I would like to thank my friends in the condensed matters physics group – Ittipon Phongkeaw, Wuttigrai Sailium, Nirawith Palagawong, Nuchalee Schwertfager, Pimpika Pimsorn, Yuwadee Suwan, and Wuttisak Prachamon for their friendships and helpful discussions. Finally, I would like to express thanks to my parents and my sister for their love, encouragement and support.

Narasak Pandech

CONTENTS

	Page
ABSTRACT IN THAI.....	I
ABSTRACT IN ENGLISH.....	II
ACKNOWLEDGEMENTS.....	III
CONTENTS.....	IV
LIST OF TABLES.....	VII
LIST OF FIGURES.....	VIII
LIST OF ABBREVIATIONS.....	X
CHAPTER	
I INTRODUCTION.....	1
1.1 Overview of the Calculations and Literature Survey.....	1
1.2 References.....	4
II THEORETICAL APPROACH.....	7
2.1 Density Functional Theory.....	7
2.1.1 The Hohenberg and Kohn Theorem.....	8
2.1.2 Kohn and Sham Equation.....	8
2.2 The Exchange Correlation Function.....	10
2.3 Bloch's Theorem and Plane Wave Basis Sets.....	12
2.4 Special k -point in the Brillouin Zone.....	14

CONTENTS (Continued)

		Page
	2.5 Pseudopotentials.....	14
	2.5.1 Norm-conserving pseudopotentials.....	17
	2.5.2 Ultrasoftpseudopotentials.....	18
	2.5.3 Projector augmented waves.....	19
	2.6 Hellmann-Feynman Theorem.....	20
	2.7 The Vienna <i>Abinitio</i> Simulation Package (VASP).....	21
	2.8 References.....	23
III	CRYSTAL PROPERTIES.....	27
	3.1 Perovskite Crystal Structure.....	27
	3.2 Elastic Properties.....	30
	3.2.1 Elastic properties of materials.....	30
	3.2.2 Elastic parameters and crystal symmetries.....	31
	3.2.3 Elastic constant calculations.....	33
	3.3 Sound Velocities in Anisotropic Materials.....	38
	3.4 References.....	44
IV	SOUND VELOCITIES AND ELASTIC PROPERTIES OF PbTiO_3	
	AND PbZrO_3 UNDER PRESSURE: FIRST PRINCIPLES STUDY.....	47
	4.1 Introduction.....	47
	4.2 Computational Method.....	48
	4.3 Results andDiscussion.....	50
	4.3.1 Structural and elastic properties.....	50

CONTENTS (Continued)

	Page
4.3.2 Elastic properties under pressure.....	52
4.4 Conclusions.....	55
4.5 References.....	55
V ELASTIC PROPERTIES OF PEROVSKITE $ATiO_3$ (A = Be, Mg, Ca, Sr and Ba) AND $PbBO_3$ (B = Ti, Zr and Hf).....	58
5.1 Introduction.....	58
5.2 Computational Methods.....	59
5.3 Results and Discussion.....	63
5.4 Conclusions.....	68
5.5 References.....	69
VI CONCLUSIONS AND FUTURE RESEARCH.....	72
6.1 Conclusions.....	72
6.2 Future Research Plan.....	73
6.3 References.....	77
APPENDIX.....	80
CURRICULUM VITAE.....	95

LIST OF TABLES

Table	Page
3.1 Atomic position in cubic perovskite.....	28
3.2 Lattice parameters for selected perovskite compounds. Our calculated values are based on the perfect cubic perovskite structure. Values in parentheses are taken from the literature.....	29
3.3 Calculated elastic constants (in GPa) for selected cubic perovskite materials. Values in parentheses are from the literature.....	37
3.4 Sound velocity expressions of each wave propagation direction for a cubic crystal.....	42
4.1 Calculated lattice constants (a) in Å, a unit cell volumes (V_0) in Å ³ , bulk modulus (B) in GPa, its pressure derivative (B'), elastic constants in GPa and sound velocities in km/s of PbTiO ₃ and PbZrO ₃ in the cubic perovskite structure compared with the literature.....	51
6.1 Atomic positions in the ideal tetragonal perovskite structure.....	75
6.2 Lattice parameters and elastic constants for selected oxides in the tetragonal perovskite structure. Values in parentheses are from the literature.....	76

LIST OF FIGURES

Figure	Page
<p>2.1 Illustrations of the pseudopotential and the pseudo wavefunction.</p> <p>The blue dash lines represent the real electrons wavefunction, $\psi(\vec{r})$, and real potential, $V(\vec{r})$. The red solid lines represent the corresponding pseudo wave functions, $\psi^{PS}(\vec{r})$ based on the pseudopotential, $V^{PS}(\vec{r})$.</p> <p>The cutoff radius, r_c represents a radius at which the all electron and pseudo quantities are matched.....</p>	16
2.2	22
<p>3.1 An ideal cubic perovskite unit cell. The dark gray spheres represent A cations, blue spheres: Bcation, and red spheres: oxygen anions.....</p>	28
3.2	33
<p>3.3 Representation of (a) the longitudinal wave and (b) the transverse wave in a slab.....</p>	40
3.4	43

LIST OF FIGURES (Continued)

Figure	Page
4.1	Elastic constants as a function of pressure for cubic perovskite PbTiO_3 and PbZrO_3 , obtained from LDA (left) and GGA (right).....53
4.2	Sound velocities as a function of pressure for cubic perovskite PbTiO_3 and PbZrO_3 , obtained from LDA (left) and GGA (right).....54
5.1	A periodic table with the cation species, used in the study, highlighted. The red rectangle highlighted the elements used on the A-site while fixing the B-site to be Ti in the cubic perovskite ABO_3 . The blue rectangle highlighted the elements used on the B-site while fixing A-site to be Pb.....61
5.2	A typical energy-strain curve fitting used to obtain the elastic constants. The black square points represent the calculated data and the red curve represents the third-degree polynomial fitting..... 62
5.3	Illustration of the polyhedral of ideal cubic perovskite crystal from (a) a perspective view and (b) top view. The blue-green cage represents the oxygen cage. The dark gray spheres represent A cations, blue-green spheres: B cation, and red spheres: oxygen anions..... 65
5.4	Elastic constants (C_{ij}) of perovskite (a) ATiO_3 and (b) PbBO_3 as a function of atomic number of A-site and B-site atom, respectively.....66
6.1	An ideal tetragonal perovskite unit cell. The dark gray spheres represent A cations, blue spheres: B cation, and red spheres: oxygen anions..... 75

LIST OF ABBREVIATIONS

DFT	= Density Functional Theory
GGA	= Generalized Gradient Approximation
LDA	= Local Density Approximation
PAW	= Projector Augmented Wave
PBE	= Perdew-Burke-Ernzerhof
PTO	= PbTiO_3
PWs	= Plane-waves
PZO	= PbZrO_3
PZT	= $\text{Pb}(\text{Zr},\text{Ti})\text{O}_3$
USPPs	= Ultra Soft Pseudo Potentials
VASP	= Vienna <i>Ab-initio</i> Simulation Package

CHAPTER I

INTRODUCTION

1.1 Overview of the Calculations and Literature Survey

The ferroelectricity of materials was discovered for the first time in Rochelle salt crystal by Valasek (Valasek, 1921). Later, the ferroelectricity was discovered in ABO_3 perovskite crystal, i.e., $BaTiO_3$ in 1945 (Kanzig, 1945), opening up a new class of materials that, later on, have successfully been used for a variety of industrial and commercial applications. In addition to ferroelectricity, there have been continued research on a wide range of interesting properties in perovskite materials, including but not limited to, piezoelectricity, semiconductivity (Samantaray *et al.*, 2004), catalytic activity (Wang *et al.*, 2007) and thermoelectricity (Frederikse *et al.*, 1964). These properties make these materials suitable for many technological applications, for e.g., eletro-optical devices, semiconductor, waveguides, laser frequency doubling, and high capacity memory cells (Wang *et al.*, 2007; Frederikse *et al.*, 1964; Auciello *et al.*, 1998; Mete *et al.*, 2003).

Because of various interesting properties of perovskite materials as mentioned above, they have been intensively investigated both theoretically and experimentally for a long time. However, there are still outstanding properties waiting to be studied as will be discussed next.

The elastic properties are among the most fundamental properties of materials that are important for their mechanical manipulation. Therefore, the elastic properties

of perovskite materials are among the properties that have been widely studied both experimentally and theoretically.

On the experimental side, the elastic properties of perovskite materials have been widely studied. For examples, Li and co-workers (Li *et al.*, 1991) used the Brillouin scattering and ultrasound techniques to measure the velocity of the ultrasound in a single tetragonal BaTiO₃ crystal. The sound velocities can be used to translate into the elastic and piezoelectric constants. Kalinichev and co-workers (Kalinichev *et al.*, 1997) also used the same method to study the elastic and piezoelectric constants of a single crystal of tetragonal PbTiO₃. The elastic properties of SrTiO₃ have also been studied by various groups using different techniques (Schranz *et al.*, 1999; Poindexter and Giardini, 1958; Lheureux *et al.*, 1999). This is because SrTiO₃ has a rather simple structure (cubic phase in nature) with high quality crystals available. Lheureux and co-worker also used the ultrasonic measurement technique to study the elastic constants and their pressure dependence of cubic SrTiO₃. In addition, they also found the cubic-tetragonal phase transition to occur at 6 GPa.

On the computation side, Wang and co-workers (Wang *et al.*, 2010) used the density functional theory (DFT) to study several properties of perovskite BaTiO₃, including the elastic properties. In their works, the elastic constants of four structures (cubic, tetragonal, orthorhombic and rhombohedral) of BaTiO₃ have been reported. Meng and co-worker (Meng *et al.*, 2010) also used DFT to study the elastic and piezoelectric properties of BaTiO₃ in the tetragonal structure. Liu and co-workers (Liu *et al.*, 2008) used DFT to study the elastic properties of perovskite PbTiO₃ in both cubic and tetragonal structures. They reported the calculated elastic constants of

both structures as well as the equilibrium tetragonal-to-cubic phase transition pressure. Their calculated transition pressure of 10.1 GPa is in a reasonable agreement with the experimental value of 11.5 ± 0.3 GPa (Zha *et al.*, 1992). The elastic properties of natural cubic perovskite SrTiO_3 have been studied by Boudali and co-workers (Boudali *et al.*, 2009). They used DFT to calculate its elastic constants. The elastic properties of another perovskite materials, SnTiO_3 , have been calculated based on DFT by Taib and co-workers (Taib *et al.*, 2012). Their results showed that SnTiO_3 is stable in the cubic phase ($\text{Pm}\bar{3}\text{m}$). Among all above mentioned theoretical studies, only the work of Taib and co-workers on SnTiO_3 , included the study of elastic properties under pressure.

Although, the elastic properties of several perovskite materials have already been studied. The knowledge on pressure dependencies of their elastic properties and sound velocities is very limited. The aim of this thesis is to employ first principles method to study the elastic properties and sound velocities of some perovskite materials under hydrostatic pressures. In this thesis, in Chapter II, we will give a brief description of the calculation method employed. In Chapter III, the calculated structural parameters under ambient conditions in comparison with available experimental and theoretical results are presented. In addition, the brief description of elasticity in materials and the elastic constants are also explained. The calculated elastic constants and sound velocities of selected cubic perovskite as a function of hydrostatic pressure are presented in Chapter IV. Because we studied various materials, we can study the trend of how the elastic constants changed with the cation species. The trends of elastic constants of ATiO_3 ($\text{A}=\text{group IIA elements}$) and PbBO_3 ($\text{B}=\text{Ti, Zr and Hf}$) are analyzed in Chapter V. Finally, the ongoing work of the elastic

properties of mentioned materials in other crystal structures are presented in Chapter VI.

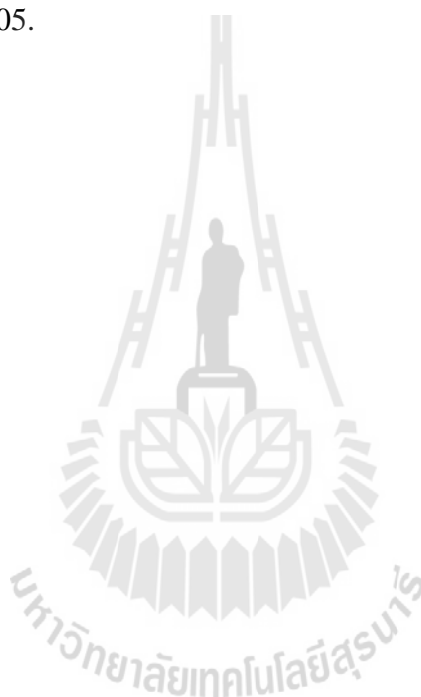
1.2 References

- Auciello, O., Scott, J. F. and Ramesh, R. (1998). The physics of ferroelectric memories. **Physics Today** 51: 22.
- Boudali, A., Khodja, M. D., Amrani, B., Bourbie, D., Amara, K. and Abada, A. (2009). First-principles study of structural, elastic, electronic, and thermal properties of SrTiO₃ perovskite cubic. **Physics Letters A** 373: 879.
- Frederikse, H. P. R., Thurber, W. R. and Hosler, W. R. (1964). Electronic transport in strontium titanate. **Physical Review** 134: A442.
- Kalinichev, A. G., Bass, J. D., Sun, B. N. and Payne, D. A. (1997). Elastic properties of tetragonal PbTiO₃ single crystals by Brillouin scattering. **Journal of Materials Research** 12: 2623.
- Kanzig, W. (1945). History of ferroelectricity 1938-1955. **Ferroelectrics** 74: 285.
- Lheureux, D., Fischer, M., Polian, A., Itie, J. P., Gauthier, M. and Syfosse, G. (1999) Elastic properties of SrTiO₃ under extreme conditions: A new high pressure ultrasonic measurement set-up. in **Ultrasonics Symposium**, 1999. Proceedings. 1999 IEEE, Vol. 1, pp. 533.
- Li, Z., Chan, S. K., Grimsditch, M. H. and Zouboulis, E. S. (1991). The elastic and electromechanical properties of tetragonal BaTiO₃ single crystals. **Journal of Applied Physics** 70: 7327.

- Liu, Y., Xu, G., Song, C., Ren, Z., Han, G. and Zheng, Y. (2008). First-principles study of elastic properties in perovskite PbTiO_3 . **Materials Science and Engineering: A** 472: 269.
- Taib M. F. M., Yaakob M. K., Chandra A., Arof A. K. and Yahya, M. Z. A. (2012). Effect of pressure on structural, electronic and elastic properties of cubic ($\text{Pm}3\text{m}$) SnTiO_3 using first principle calculation. **Advanced Materials Research** 501: 342.
- Meng, X., Wen, X. and Qin, G. (2010). DFT study on elastic and piezoelectric properties of tetragonal BaTiO_3 . **Computational Materials Science** 49: S372.
- Mete, E., Shaltaf, R. and Ellialtıođlu, Ő. (2003). Electronic and structural properties of a 4d perovskite: Cubic phase of SrZrO_3 . **Physical Review B** 68: 035119.
- Poindexter, E. and Giardini, A. A. (1958). Elastic constants of strontium titanate (SrTiO_3). **Physical Review** 110: 1069.
- Samantaray, C. B., Sim, H. and Hwang, H. (2004). Electronic structure and optical properties of barium strontium titanate ($\text{Ba}_x\text{Sr}_{1-x}\text{TiO}_3$) using first-principles method. **Physica B: Condensed Matter** 351: 158.
- Schranz, W., Sondergeld, P., Kityk, A. V. and Salje, E. K. H. (1999). Elastic properties of SrTiO_3 crystals at ultralow frequencies. **Phase Transitions** 69: 61.
- Valasek, J. (1921). Piezo-electric and allied phenomena in rochelle salt. **Physical Review** 17: 475.
- Wang, H., Wang, B., Li, Q., Zhu, Z., Wang, R. and Woo, C. H. (2007). First-principles study of the cubic perovskites BiMO_3 ($\text{M}=\text{Al}$, Ga , In , and Sc). **Physical Review B** 75: 245209.

Wang, J. J., Meng, F. Y., Ma, X. Q., Xu, M. X. and Chen, L. Q. (2010). Lattice, elastic, polarization, and electrostrictive properties of BaTiO_3 from first-principles. **Journal of Applied Physics** 108: 034107.

Zha, C. S., Kalinichev, A. G., Bass, J. D., Suchicital, C. T. A. and Payne, D. A. (1992). Pressure dependence of optical absorption in PbTiO_3 to 35 GPa: Observation of the tetragonal-to-cubic phase transition. **Journal of Applied Physics** 72: 3705.



CHAPTER II

THEORETICAL APPROACH

For simulation of materials, various information of materials system could be extracted from the electron wave function. In principle, the electron wave function can be obtained by solving the Schrödinger equation of the many-electron system. However, directly solving the full set of Schrödinger equations of many-electron problem is too complicated. Hence, there are many approximations employed to simplify the many body problems into solvable ones. The density functional theory (DFT) is the widely used method to reduce the many-electron Schrödinger equation into a solvable problem. In this chapter, we will briefly explain the theories, approximations, methods and software used in this thesis. Detailed information can be found in the respective literature referenced throughout the chapter.

2.1 Density Functional Theory

The success of DFT is not limited to standard bulk materials, but also for complex materials such as proteins and carbon nanotube (Ramachandran *et al.*, 2008). The main idea of DFT is to describe the complicated many-body electron interactions through its density, $n(\vec{r})$ (Parr and Yang, 1989), not its wavefunction, ψ_i . DFT can be viewed as a ground state theory with the electron charge density serving as the

variational parameter (Hohenberg and Kohn, 1964). The description in detail of DFT will be described in the following section.

2.1.1 The Hohenberg and Kohn Theorem

For any system consisting of electrons moving under the external potential, $V_{ext}(\vec{r})$, Hohenberg and Kohn proposed that the ground state energy and all properties of electron wavefunction in the external potential can be determined from the electron density, $n(\vec{r})$. They showed the ground-state energy of many electron wavefunction can be written as (Hohenberg and Kohn, 1964)

$$E[n(\vec{r})] = \int V_{ext}(\vec{r})n(\vec{r})d^3r + F[n(\vec{r})], \quad (2.1)$$

where $V_{ext}(\vec{r})$ is the external potential which generated by the interaction between nuclei and electrons. $F[n(\vec{r})]$ is an unknown function, but it is a universal functional of the electron density $n(\vec{r})$. It does not depend on the external potential and includes all kinetic energy and electron-electron interaction terms (Parr and Yang, 1989).

2.1.2 Kohn and Sham Equation

Kohn and Sham (Kohn and Sham, 1965) introduced a method based on Hohenberg and Kohn theorems to minimize the ground state energy function. They proposed that the universal function ($F[n(\vec{r})]$) in Equation 2.1 can be separated into three parts. Therefore, the ground-state energy of many electron wavefunction can be written as,

$$E[n(\bar{r})] = \int V_{ext}(\bar{r})n(\bar{r})d^3r + V_H[n(\bar{r})] + T_s[n(\bar{r})] + E_{xc}[n(\bar{r})], \quad (2.2)$$

where the second term, $V_H[n(\bar{r})]$, is the electron-electron Coulomb energy (also often referred to as Hartree energy) can be defined as,

$$V_H = \frac{e^2}{2} \iint \frac{n(\bar{r})n(\bar{r}')}{|\bar{r}-\bar{r}'|} d^3r d^3r'. \quad (2.3)$$

The third term, $T_s[n(\bar{r})]$ is the kinetic energy of the non-interacting system with the same density and it is not the exact kinetic energy function ($T[n(\bar{r})]$). The difference between $T[n(\bar{r})]$ and $T_s[n(\bar{r})]$ is proposed to be small and can be included into the exchange-correlation energy, $E_{xc}[n(\bar{r})]$ which is the last term in Equation 2.2 (Parr and Yang, 1989).

Therefore, the Kohn-Sham-effective potential can be written as,

$$V_{eff}(\bar{r}) = V_{ext}(\bar{r}) + e^2 \int \frac{n(\bar{r}')}{|\bar{r}-\bar{r}'|} d^3r' + \frac{\delta E_{xc}[n(\bar{r})]}{\delta n}. \quad (2.4)$$

Finally, the ground state solution of a one-particle problem can be obtained by solving the Schrödinger equation in the effective potential $V_{eff}(\bar{r})$,

$$\left[-\frac{\hbar^2}{2m} \nabla^2 + V_{eff}(\bar{r}) \right] \psi_i(\bar{r}) = \varepsilon_i \psi_i(\bar{r}). \quad (2.5)$$

The electron density for this system is given by (Kohn and Sham, 1965),

$$n(\bar{r}) = \sum_{i=1}^N |\psi_i(\bar{r})|^2, \quad (2.6)$$

where N is the number of electrons.

Equation 2.5 has to be solved self-consistently. Initially, a guess of $n(\vec{r})$ is used to construct V_{eff} , which is an important function needed to define the Schrödinger equation in Equation 2.5. The Schrödinger equation then can be solved to obtain the wavefunctions ψ_i . Then the so-obtained ψ_i can be used to construct an improved $n(\vec{r})$. The improved $n(\vec{r})$ is then used to construct new V_{eff} in Equation 2.5. This routine is repeated until convergence is reached, i.e., the $n(\vec{r})$ remains unchanged (or changed between the iterations within an acceptable value).

2.2 The Exchange Correlation Function

In Equation 2.4, the exchange correlation energy $E_{xc}[n(\vec{r})]$ is the only part in the effective potential (V_{eff}), which is not exactly known. In order to solve the one-particle Schrödinger equation in Equation 2.5, the $E_{xc}[n(\vec{r})]$ must be approximated or defined. In this thesis, two popular approximations of $E_{xc}[n(\vec{r})]$ were employed; the local density approximation (LDA) and the generalized gradient approximation (GGA).

LDA, which was introduced by Kohn and Sham in 1965 (Kohn and Sham, 1965), can be said to be the most widely used approximation. It is assumed that the density can be treated locally as a uniform electron gas. Under LDA, the $E_{xc}[n(\vec{r})]$ depends on the value of electron density at each point in the system. The local density approximation defines the exchange correlation energy as (Parr and Yang, 1989),

$$E_{xc}^{LDA} [n(\vec{r})] = \int n(\vec{r}) \varepsilon_{xc} [n(\vec{r})] d^3r, \quad (2.7)$$

where $\varepsilon_{xc} [n(\vec{r})]$ is the exchange correlation energy per particle of a homogeneous electron gas with the density $n(\vec{r})$. The $\varepsilon_{xc} [n(\vec{r})]$ can be written in the combination between exchange and correlation energy as (Parr and Yang, 1989),

$$\varepsilon_{xc} [n(\vec{r})] = \varepsilon_x [n(\vec{r})] + \varepsilon_c [n(\vec{r})], \quad (2.8)$$

where $\varepsilon_x [n(\vec{r})]$ and $\varepsilon_c [n(\vec{r})]$ are the exchange and correlation energy density of a homogeneous electron gas of density $n(\vec{r})$, respectively. The exchange energy term, $\varepsilon_x [n(\vec{r})]$ was derived from the analytical form of a homogeneous electron gas by Dirac in 1930 (Dirac, 1930) and can be written as (Parr and Yang, 1989),

$$\varepsilon_x [n(\vec{r})] = -C_x n(\vec{r})^{1/3}, \quad C_x = \frac{3}{4} \left(\frac{3}{\pi} \right)^{1/3}. \quad (2.9)$$

The correlation energy term, $\varepsilon_c [n(\vec{r})]$ was first calculated by Wigner (Wigner, 1938). For a homogeneous electron gas at different densities, the correlation energy was calculated based on quantum Monte Carlo calculations by Ceperley and Alder (Ceperley and Alder, 1980). The LDA method was successfully used for calculating the equilibrium structures and harmonic vibration frequencies of crystals but it usually fails in obtaining an accurate binding energy. Details of successes and failures of LDA have been nicely discussed by Jones and Gunnarsson (Jones and Gunnarsson, 1989).

Later GGA was introduced to take into account the variation of electron density in space. Under GGA, the exchange-correlation energy $E_{xc} [n(\vec{r})]$ is a function of the electron densities and their gradients, $|\nabla n(\vec{r})|$ (Kohn, 1999).

$$E_{xc}^{GGA} [n(\vec{r})] = \int f [n(\vec{r}), \nabla n(\vec{r})] n(\vec{r}) d^3 r. \quad (2.10)$$

GGA method improves the ground state properties. It reduces the errors in the binding energy of light atoms, especially in small molecules. For solids, GGA usually produces larger equilibrium lattice parameters than LDA and it is not clear which one is better in a particular system than the other. In many cases, GGA overcorrects the LDA results, leading to the results are in worse agreement with experiments. However, GGA is believed to provide improved the value of binding energies, especially, for the systems that the electron density is more fluctuated.

There are many forms of GGA functional for the exchange correlation energy, $E_{xc} [n(\vec{r})]$. The popularly used are B88 (Becke, 1988), PW91 (Perdew and Wang, 1992), and PBE (Perdew *et al.*, 1996).

2.3 Bloch's Theorem and Plane Wave Basis Sets

Even with the DFT and a simple exchange-correlation function, the direct calculation of an almost infinite number of electrons in the electric field from an almost infinite number of ions is still impossible. In a direct calculation of a real system, the wave function has to be calculated for each and every electron in the system which is in the order of 10^{23} electrons. In addition, to fully describe each electron wave function, the basis set, if not carefully chosen, could be infinitely large.

However, the fact that crystalline has periodicity of ions can be used to reduce the computational demand based on Bloch's theorem. By using this theorem, it is possible to express the wave function of an infinite crystal in terms of the wave functions in the reciprocal space.

In principle, Bloch's theorem uses the periodicity of a crystal to transform the real space electron wave functions to the reciprocal space wave functions. Bloch's plane wave function can be written as a product of the wave part, $e^{i\vec{k}\cdot\vec{r}}$ and a periodic part, $u_{n\vec{k}}(\vec{r})$ (Kittel, 1996),

$$\psi_{n\vec{k}}(\vec{r}) = e^{i\vec{k}\cdot\vec{r}} u_{n\vec{k}}(\vec{r}), \quad (2.11)$$

where

$$u_{n\vec{k}}(\vec{r}) = u_{n\vec{k}}(\vec{r} + \vec{R}). \quad (2.12)$$

Equation 2.11 and 2.12 are the well-known Bloch's theorem, where \vec{r} is the position in the crystal, \vec{R} is the lattice translation vector in the crystal, \vec{k} is the wave vector, n is the band index representing different solutions that have the same wave vector \vec{k} . Using the Fourier transformation of the periodic function to the reciprocal space, the wave function in Equation 2.11 can be written in the sum plane waves form as (Kittel, 1996),

$$\psi_{n\vec{k}}(\vec{r}) = \sum_{\vec{G}} u_{n\vec{k}}(\vec{G}) e^{i(\vec{k}+\vec{G})\cdot\vec{r}}, \quad (2.13)$$

where \vec{G} is the reciprocal lattice vectors. This allows the calculations to be done in the reciprocal space. In order to limit the number of plane wave used for the expansion, the plane waves used in the calculations are those with the kinetic energy smaller than the energy cutoff, E_{cutoff} , (Martin, 2004),

$$\frac{\hbar^2}{2m}|k + G|^2 < E_{cutoff}. \quad (2.14)$$

The value of required energy cutoff depends on the required accuracy of the results and the complication of the wave functions which is mainly related to the elements under study.

2.4 Special k-point in the Brillouin Zone

The Brillouin zone is the Wigner-Seitz cell in the reciprocal lattice, which is defined by the planes that are the perpendicular bisectors of the vectors from the origin to the reciprocal lattice points. The first Brillouin zone is the smallest unit cell in the reciprocal space that corresponds to the crystal unit cell in real space (Martin, 2004). In principle, we should calculate for the wave functions at every k-point in the first Brillouin zone. In practice, it is impossible to do calculations with the infinite number of k-points and the wavefunctions are quite similar for k-points in the same vicinity. Therefore, it is possible to sampling a limited number of k-points in the first Brillouin zone. There are various k-point sampling methods introduced. In this work, we employed the sampling method introduced by Monkhorst and Pack (Monkhorst and Pack, 1976)

2.5 Pseudopotentials

Electrons in materials can be divided into two types: core electrons and valence electrons. The core electrons are in the inner shell of each atom. The valence electrons are in the outer shell. The valence-electron wavefunctions are orthogonal to the core-electron wavefunctions. A set of plane-waves (PWs) with a limited E_{cutoff} is

not suitably to describe the core region. This is because the wavefunctions in the core region has a fast oscillation characteristic (Heine *et al.*, 1970). However, the physical properties of materials depend mainly on the valence electrons. Therefore, pseudopotential approach was introduced. In the pseudopotential approach, the core electrons are approximated to be “frozen”. The valence-electron wavefunctions do not need to be orthogonal to the core states. This means that the properties of the systems are calculated based on an assumption that core electrons are not involved in the chemical bonding and do not change as a result of structural modifications. In the pseudopotential scheme, the deep core potential part is replaced by a smooth pseudopotential, $V^{PS}(\vec{r})$ as illustrated in Figure 2.1. Removing the core electrons from the calculations should not seriously affect the bonding properties in materials because the core electrons should remain almost unchanged under all deformations of interest shall it be included. The corresponding set of pseudo wavefunctions, $\psi^{PS}(\vec{r})$ and all electron wavefunctions, $\psi(\vec{r})$ are matched outside a selected core radius, r_c . Inside r_c , $\psi^{PS}(\vec{r})$ does not have the fast oscillation features that required the plane waves with high energy cutoff to describe. Instead, the wave function which is the solution to pseudopotential becomes very smooth in core area as illustrated in Figure 2.1.

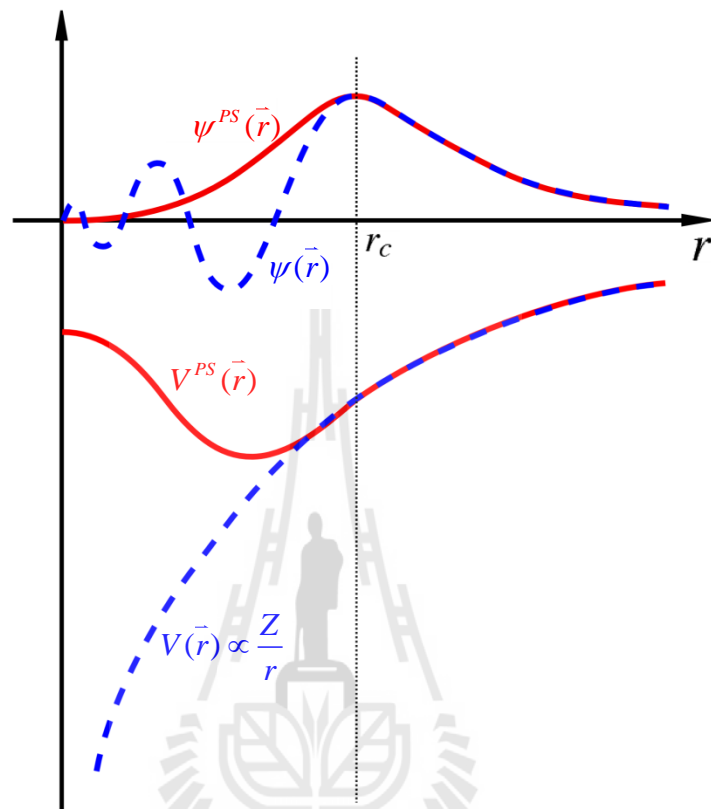


Figure 2.1 Illustrations of the pseudopotential and the pseudo wavefunction. The blue dash lines represent the real electrons wavefunction, $\psi(\vec{r})$, and real potential, $V(\vec{r})$. The red solid lines represent the corresponding pseudo wave functions, $\psi^{PS}(\vec{r})$ based on the pseudopotential, $V^{PS}(\vec{r})$. The cutoff radius, r_c represents a radius at which the all electron and pseudo quantities are matched. (The figure is reproduced from Ref. (Wolfram Quester Source, 2006))

2.5.1 Norm-conserving pseudopotentials

Initially one of the requirements of the pseudopotentials is the norm-conserving conditions. This is to ensure that the integration of both pseudo and all-electron wavefunctions within the core region be the same (Hamann *et al.*, 1979). The norm-conserving conditions are defined from the following list of conditions (Martin, 2004).

1. Outside the core, the real and pseudo wavefunctions generate the same charge density, this can be expressed as,

$$\int_0^{r_c} \psi_{AE}^*(\vec{r}) \psi_{AE}(\vec{r}) d^3\vec{r} = \int_0^{r_c} \psi_{PS}^*(\vec{r}) \psi_{PS}(\vec{r}) d^3\vec{r} . \quad (2.15)$$

Equation 2.15 means that all electron and pseudo wavefunctions (should be smooth and nodeless) are the same outside the core, i.e.,

$$\psi_{AE}(\vec{r}) = \psi_{PS}(\vec{r}) ; r > r_c . \quad (2.16)$$

2. The eigenvalues should be conserved, i.e.,

$$\varepsilon^{AE} = \varepsilon^{PS} . \quad (2.17)$$

3. The logarithmic derivatives of all electron and pseudo wavefunctions and their first energy derivatives agree at r_c .

The logarithmic derivative for an angular momentum l , can be written as

$$D_l(\varepsilon) = \left. \frac{d}{dr} \ln \psi_l(r; \varepsilon) \right|_{r_c} = \frac{\psi_l'(r; \varepsilon)}{\psi_l(r; \varepsilon)} , \quad (2.18)$$

where $\psi_l(r; \varepsilon)$ is the solution of the radial Kohn-Sham equation for a fixed potential and fixed energy ε .

The norm-conserving pseudopotentials, V^{PS} can be divided into the local potential, ($V_{loc}^{PS}(r)$) and the non-local potential, ($V_{nonloc}^{PS}(r)$) (Kleinman and Bylander, 1982) as,

$$V^{PS} = V_{loc}^{PS}(r) + V_{nonloc}^{PS}(r) = V_{loc}^{PS}(r) + \sum_l |\beta_l\rangle V_l \langle \beta_l|. \quad (2.19)$$

The non-local part is the deviation from the all electron potential and is confined inside r_c . The projector, $|\beta_l\rangle$ acts on the wavefunctions with angular momentum (l), which is localized within r_c .

2.5.2 Ultrasoft pseudopotentials

Although pseudopotentials allows the expansion of pseudo wavefunctions using a set of plane waves as a basis, there are still quite a large number of plane waves required to produce an accurate wave functions. Small increase in number of plane waves used in the basis set significantly impact the computation demand. To reduce number of plane waves needed, an ultrasoft pseudopotentials (USPPs) approach were introduced. The USPPs approach was introduced by Vanderbilt in 1990 (Vanderbilt, 1990), in order to allow the calculations to be performed with the lowest possible cutoff energy for the plane-wave basis set.

The norm-conserving requirements have been relaxed in USPPs, to obtain shallower potentials and smoother wave functions in the core regions. Instead of using the plane wave to describe the full valence electron wave function, only small portion of the wave function is calculated within the USPPs scheme. This allows one to reduce substantially the wave cutoff energy in the calculations (Meyer, 2006).

2.5.3 Projector augmented waves

The projector augmented waves (PAW) method was proposed by Blöchl (Blöchl, 1994). In this method, a smooth wavefunction (ψ) is created. There exists a linear transformation which relates the all electron wave function (ψ) to the smooth wavefunction (ψ) by the linear transformation operator, τ through the relationship,

$$|\psi\rangle = \tau |\psi\rangle. \quad (2.20)$$

Utilizing the linear transformation of PAW method, the all electron wavefunction (ψ) can be written as

$$|\psi\rangle = |\psi\rangle + \sum_m (|\psi_m\rangle - |\psi_m\rangle) \langle p_m | \psi \rangle, \quad (2.21)$$

where ψ_m is the localized all electron partial wave for state m , ψ_m is the localized smooth partial wave for state m , and $\langle p_m |$ is the localized projection operator. The linear transformation operator τ can be written as,

$$\tau = 1 + \sum_m (|\psi_m\rangle - |\psi_m\rangle) \langle p_m |. \quad (2.22)$$

In Equation 2.22, the linear transformation operator τ can be used to add back the core potential of an all electron wavefunction to a smoothed wavefunction. Note that Equation 2.22 can be for core as well as valence states (Martin, 2004).

2.6 Hellmann-Feynman Theorem

The Hellmann-Feynman theorem derives from the relationship between the derivative of the total energy and the derivation of the Hamiltonian. If λ is a parameter in the Hamiltonian, (H), we can write the derivative of energy with respect to λ as

$$\begin{aligned}\frac{\partial E}{\partial \lambda} &= \frac{\partial}{\partial \lambda} \langle \psi | H | \psi \rangle = \left\langle \frac{\partial \psi}{\partial \lambda} | H | \psi \right\rangle + \left\langle \psi | \frac{\partial H}{\partial \lambda} | \psi \right\rangle + \left\langle \psi | H | \frac{\partial \psi}{\partial \lambda} \right\rangle, \\ \frac{\partial E}{\partial \lambda} &= E \left\langle \frac{\partial \psi}{\partial \lambda} | \psi \right\rangle + \left\langle \psi | \frac{\partial H}{\partial \lambda} | \psi \right\rangle + E \left\langle \psi | \frac{\partial \psi}{\partial \lambda} \right\rangle, \\ \frac{\partial E}{\partial \lambda} &= E \frac{\partial}{\partial \lambda} \langle \psi | \psi \rangle + \left\langle \psi | \frac{\partial H}{\partial \lambda} | \psi \right\rangle, \\ \frac{\partial E}{\partial \lambda} &= \left\langle \psi | \frac{\partial H}{\partial \lambda} | \psi \right\rangle, \tag{2.23}\end{aligned}$$

where $\psi(\lambda)$ is an eigenfunction of H . Equation 2.23 is the well-known Hellmann-Feynman theorem (Hellmann, 1937). It shows that the derivative of the total energy with respect to a parameter λ can be calculated using the derivative of the operator instead. If λ is \mathbf{R} , the forces are obtained and the Hellmann-Feynman force theorem is written as,

$$F_i = -\frac{\partial E}{\partial R_i} = -\int n(\vec{r}) \frac{\partial V_{ext}(\vec{r})}{\partial R_i} d^3 \vec{r} - \frac{\partial E_{II}}{\partial R_i} = -\left\langle \psi | \frac{\partial H}{\partial R_i} | \psi \right\rangle - \frac{\partial E_{II}}{\partial R_i}, \tag{2.24}$$

where E_{II} is the electrostatic nucleus-nucleus (ion-ion) interaction.

2.7 The Vienna *Ab initio* Simulation Package (VASP)

In this thesis, the calculations were performed by using the Vienna *Ab initio* Simulation Package (VASP) developed by Kresse, Hafner and Furthmüller (Kresse and Hafner, 1994; Kresse and Furthmüller, 1996a; Kresse and Furthmüller, 1996b). In VASP, the electron wavefunctions are described by using the planewaves (PWs) basis set. The ultrasoft pseudopotentials (USPPs) (Vanderbilt, 1990) and projector augmented wave (PAW) (Blöchl, 1994) potentials needed for the calculations are included in package. In this thesis, the pseudopotentials (without PAW) that are sufficient to provide good description of elastic properties are mainly employed. The k-point samplings are based on the Monkhorst-Pack approach (Monkhorst and Pack, 1976). The main computational part for solving the Kohn-Sham equation self-consistently utilized an iterative matrix-diagonalization scheme such as, a conjugate gradient scheme (Teter *et al.*, 1989; Bylander *et al.*, 1990) and block Davidson scheme (Davidson, 1983). The Broyden/Pulay mixing scheme (Pulay, 1980; Johnson, 1988) is efficiency used for mixing the original and new electronic charge density during the self-consistency calculation loops. The computational scheme used by the VASP codes is illustrated in Figure 2.2. More details can be found in the manual of VASP (Kresse and Furthmüller, 2012) and an article by the developers (Kresse and Hafner, 1994; Kresse and Furthmüller, 1996b).

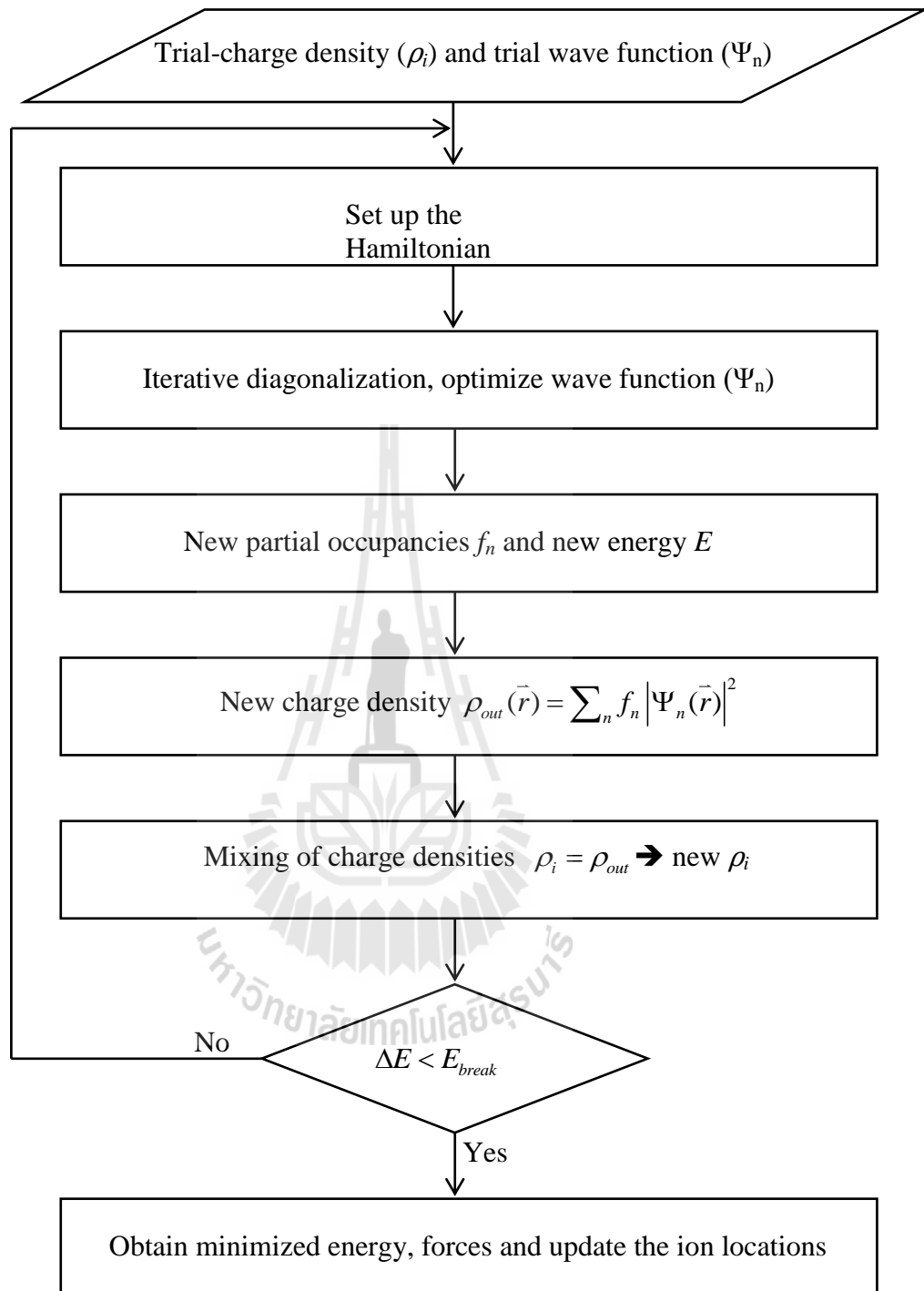


Figure 2.2 The self-consistency scheme used in the VASP codes.

2.8 References

- Becke, A. D. (1988). Correlation energy of an inhomogeneous electron gas: A coordinate-space model. **The Journal of Chemical Physics** 88: 1053.
- Blöchl, P. E. (1994). Projector augmented-wave method. **Physical Review B** 50: 17953.
- Blöchl, P. E. (1994). Projector augmented-wave method. **Physical Review B** 50: 17953.
- Bylander, D. M., Kleinman, L. and Lee, S. (1990). Self-consistent calculations of the energy bands and bonding properties of B₁₂C₃. **Physical Review B** 42: 1394.
- Ceperley, D. M. and Alder, B. J. (1980). Ground state of the electron gas by a stochastic method. **Physical Review Letters** 45: 566.
- Davidson, E. R. (1983). **Methods in Computational Molecular Physics** edited by **Dierksen, G. H. F. and Wilson**. New York: Plenum.
- Dirac, P. A. M. (1930). Note on exchange phenomena in the thomas atom. **Mathematical Proceedings of the Cambridge Philosophical Society** 26: 376.
- Hamann, D. R., Schlüter, M. and Chiang, C. (1979). Norm-conserving pseudopotentials. **Physical Review Letters** 43: 1494.
- Heine, V., Cohen, M. L. and Weaire, D. (1970). **Solid State Physics**. edited by **Ehrenreich, H. E., Seitz, F., and Turnbull, D**. New York: Academic press.
- Hellmann, H. (1937). **Einführung in die Quantumchemie**. Leipzig: Deutsche.
- Hohenberg, P. and Kohn, W. (1964). Inhomogeneous electron gas. **Physical Review** 136: B864.

- Johnson, D. D. (1988). Modified Broyden's method for accelerating convergence in self-consistent calculations. **Physical Review B** 38: 12807.
- Jones, R. O. and Gunnarsson, O. (1989). The density functional formalism, its applications and prospects. **Reviews of Modern Physics** 61: 689.
- Kittel, C. (1996). **Introduction to Solid State Physics**. United State of America: Cambridge University. John Wiley & Sons, Inc.
- Kleinman, L. and Bylander, D. M. (1982). Efficacious form for model pseudopotentials. **Physical Review Letters** 48: 1425.
- Kohn, W. (1999). Nobel Lecture: Electronic structure of matter—wave functions and density functionals. **Reviews of Modern Physics** 71: 1253.
- Kohn, W. and Sham, L. J. (1965). Self-Consistent equations including exchange and correlation effects. **Physical Review** 140: A1133.
- Kresse, G. and Furthmüller, J. (1996a). Efficiency of *ab-initio* total energy calculations for metals and semiconductors using a plane-wave basis set. **Computational Materials Science** 6: 15.
- Kresse, G. and Furthmüller, J. (1996b). Efficient iterative schemes for ab initio total-energy calculations using a plane-wave basis set. **Physical Review B** 54: 11169.
- Kresse, G. and Furthmüller, J. (2012). **Vienna *ab-initio* simulation package: VASP the GUIDE**. Wien: Institut für Materialphysik, Universität Wien.
- Kresse, G. and Hafner, J. (1994). Norm-conserving and ultrasoft pseudopotentials for first-row and transition elements. **Journal of Physics: Condensed Matter** 6: 8245.

- Martin, R. M. (2004). **Electronic Structure: Basic Theory and Practical Methods**.
United Kingdom: Cambridge University Press.
- Meyer, B. (2006). The pseudo plane wave approach. **John von Neumann Institute for Computing** 31: 71.
- Monkhorst, H. J. and Pack, J. D. (1976). Special points for Brillouin-zone integrations. **Physical Review B** 13: 5188.
- Parr, G. R. and Yang, W. (1989). Density-Functional theory of atoms and molecules.
The United States of America: Oxford University Press.
- Perdew, J. P., Burke, K. and Ernzerhof, M. (1996). Generalized gradient approximation made simple. **Physical Review Letters** 77: 3865.
- Perdew, J. P. and Wang, Y. (1992). Accurate and simple analytic representation of the electron-gas correlation energy. **Physical Review B** 45: 13244.
- Pulay, P. (1980). Convergence acceleration of iterative sequences the case of SCF iteration. **Chemical Physics Letters** 73: 393.
- Ramachandran, K. I., Deepa, G. and Namboori, K. (2008) Density functional theory. in computational chemistry and molecular modeling Springer Berlin Heidelberg, pp. 171.
- Teter, M. P., Payne, M. C. and Allan, D. C. (1989). Solution of Schrodinger's equation for large systems. **Physical Review B** 40: 12255.
- Vanderbilt, D. (1990). Soft self-consistent pseudopotentials in a generalized eigenvalue formalism. **Physical Review B** 41: 7892.
- Wigner, E. (1938). Effects of the electron interaction on the energy levels of electrons in metals. **Transactions of the Faraday Society** 34: 678.

Wolfram Quester Source (2006). [On-line] Available:

[http://en.wikipedia.org/wiki/File: SketchPseudopotentials.png](http://en.wikipedia.org/wiki/File:SketchPseudopotentials.png).



CHAPTER III

CRYSTAL PROPERTIES

3.1 Perovskite Crystal Structure

The family of perovskite materials is composed of a large number of compounds. The ideal cubic perovskite (space group $Pm\bar{3}m$) structure has ABX_3 stoichiometry and is composed of a three-dimensional framework of corner-sharing AB_6 octahedra. The structure of an ideal cubic perovskite is illustrated in Figure 3.1, where the A cations are located at the corners of the cube. B cation is located in the center of oxygen cage, where the oxygen ions located at the face-centered position of the cube. The A-site cation fills the 12-fold coordination formed by the BX_3 network and is surrounded by 12 equidistant anions (Johnsson and Lemmens, 2007). The ideal cubic perovskite structure is simple but not the commonly observed structure. The observed structures usually involves the tilting of BX_6 octahedra, the displacement of B-site cations, and/or the distortion of the octahedral (Megaw, 1973). Additionally, if either or both of the A- and B-cation sites contain more than one cation types (including vacancies), an ordering of A cations and/or B cations may occur, resulting in the distortion from the cubic symmetry (Mitchell, 2002; C.J. Howard *et al.*, 2003; Howard and Stokes, 2002). The distortion is directly related to the physical properties of these compounds. Recently, the perovskite oxide family (ABO_3) is widely studied. In this thesis, we focus our attentions on the $ATiO_3$ perovskite materials (where A is a divalent metal) and $PbBO_3$ perovskite materials (where $B = Ti, Zr$ and Hf).

Although the actual structure of some studied compounds might have some distortion from the ideal cubic structure, for simplicity, only the perfect cubic structure is chosen in this thesis. The equivalent positions of the atoms are shown in Table 3.1. The calculated values of lattice parameters for selected perovskite materials are shown in Table 3.2 in comparison with available calculated and experimental results in the literatures. Our calculated values are in good agreement with the literatures.

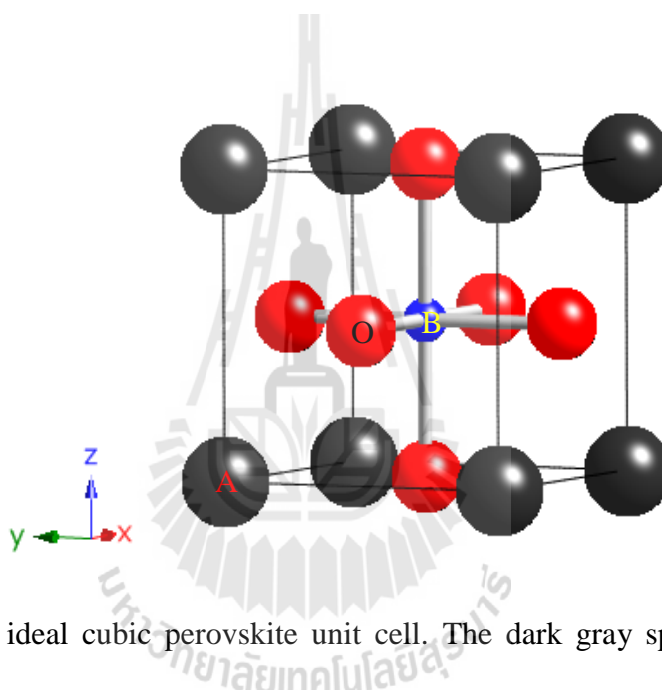


Figure 3.1 An ideal cubic perovskite unit cell. The dark gray spheres represent A cations, blue spheres: B cation, and red spheres: oxygen anions.

Table 3.1 Atomic positions in cubic perovskite.

Site	Location	Co-ordinations
A cation	(2a)	(0, 0, 0)
B cation	(2a)	(0.5, 0.5, 0.5)
O anion	(6b)	(0.5, 0.5, 0) (0.5, 0, 0.5) (0, 0.5, 0.5)

Table 3.2 Lattice parameters for selected perovskite compounds. Our calculated values are based on the perfect cubic perovskite structure. Values in parentheses are taken from the literature.

Materials	Parameters	Calculations		Expt.
		LDA	GGA	
BeTiO ₃	a (Å)	3.76	3.82	-
	V (Å ³)	53.2	55.7	
MgTiO ₃	a (Å)	3.79	3.84	-
	V (Å ³)	54.4	56.6	
CaTiO ₃	a (Å)	3.82 (3.89 ^a)	3.88	(3.90 ^b , 3.895 ^c)
	V (Å ³)	55.7	58.4	
SrTiO ₃	a (Å)	3.87 (3.86 ^d , 3.91 ^h)	3.94 (3.94 ^e)	(3.92 ^e)
	V (Å ³)	58.0	61.2	
BaTiO ₃	a (Å)	3.95 (4.00 ^f , 3.96 ^d)	4.02 (4.03 ^d)	4.00 ^g
	V (Å ³)	61.6	65.0	
SnTiO ₃	a (Å)	3.87 (3.89 ⁱ)	3.94 (3.94 ⁱ)	-
	V (Å ³)	58.0	61.2	
PbTiO ₃	a (Å)	3.89 (3.93 ^d)	3.97 (3.96 ^d)	(3.97 ^j)
	V (Å ³)	58.9	62.57	
PbZrO ₃	a (Å)	4.13 (4.11 ^k)	4.19 (4.19 ^k , 4.18 ^l)	(4.16 ^m)
	V (Å ³)	70.4	73.56	
PbHfO ₃	a (Å)	4.08	4.14	-
	V (Å ³)	68.0	71.0	

^aCalculations by Lee *et al.* (Lee *et al.*, 2009)

^bMeasurement by Ali and Yashima (Ali and Yashima, 2005)

^cMeasurement by Brendan *et al.* (Brendan *et al.*, 1999)

^dCalculations by Piskunov *et al.* (Piskunov *et al.*, 2004)

^eCalculations by Boudali *et al.* (Boudali *et al.*, 2009)

^fCalculations by Wang *et al.* (Wang *et al.*, 2010)

^gMeasurement by Hellwage *et al.* (K.H. Hellwage and A.M. Hellwage, 1969)

^hCalculations by Daga *et al.* (Avinash Daga *et al.*, 2011)

ⁱCalculations by Parker *et al.* (Parker *et al.*, 2011)

^jMeasurement by Shirane *et al.* (Shirane *et al.*, 1956)

^kCalculations by Wang *et al.* (Wang *et al.*, 2005)

^lCalculations by Baedi *et al.* (Baedi *et al.*, 2008)

^mMeasurement by Fujishita *et al.* (Fujishita *et al.*, 2002)

3.2 Elastic Properties

For material developments, elastic properties of materials have been intensively studied. They are the fundamental important information for interpreting and understanding the nature of bonding in solid and can be used to describe the material mechanical behaviors. In this section we will give a brief introduction to the theory of elastic properties of materials and the set up to calculate them.

3.2.1 Elastic properties of materials

A solid object under an external force is in a state of stress. The stress is defined as the force per unit area. Because force is a vector quantity, the stress is a direction dependent quantity and generally described by a stress tensor σ_{ij} . If all parts of the object are in equilibrium and no external force, the Einstein's convention equation for summation (Kittel, 1996) can be written as

$$\frac{\partial \sigma_{ij}}{\partial x_j} = 0, \quad (3.1)$$

where x_j denoted as the Cartesian axes. The deformations of the object caused by the external stress are described by the strain tensor e_{ij} . If an atom is displaced with the displacements u_i , the strain tensor is defined as

$$e_{ij} = \frac{1}{2} \left(\frac{\partial u_i}{\partial x_j} + \frac{\partial u_j}{\partial x_i} \right). \quad (3.2)$$

In the strain tensor, the diagonal components (e_{11} , e_{22} and e_{33}) are called tensile strain, whereas the off-diagonal components are called shear strain. For a small deformation, the linear theory of elasticity is a good approximation of the strained state of solid. For small stresses (or small deformations), the elongations and distortions of an object

are generally linearly proportional to the applied stresses. Note, however, that this theoretical model does not refer to the atomistic nature of the matter, i.e., the atomic bonds or the crystal structures do not enter as a prerequisite to this concept. The range of the linearity is called the *elastic limit*. Beyond the elastic limit, a non-linear effect can break the direct proportional between the stress and strain, this region is called *plastic region*. For large stresses, a plastic dissipation makes the deformation irreversible (Kittel, 1996).

3.2.2 Elastic parameters and crystal symmetries

The elastic parameters are the fundamental parameters providing detailed information on the mechanical properties of the materials. These qualities can give insight on the mechanical behaviors of the material under different situations. Based on Hook's law for solid with a small deformation, stress components, σ_{ij} ($i, j = x, y, z$), can be expressed in term of the strain components, e_{ij} ($i, j = x, y, z$) in the matrix form as (Elliott, 1998),

$$\begin{pmatrix} \sigma_{xx} \\ \sigma_{yy} \\ \sigma_{zz} \\ \sigma_{yz} \\ \sigma_{zx} \\ \sigma_{xy} \end{pmatrix} = \begin{pmatrix} C_{11} & C_{12} & C_{13} & C_{14} & C_{15} & C_{16} \\ C_{21} & C_{22} & C_{23} & C_{24} & C_{25} & C_{26} \\ C_{31} & C_{32} & C_{33} & C_{34} & C_{35} & C_{36} \\ C_{41} & C_{42} & C_{43} & C_{44} & C_{45} & C_{46} \\ C_{51} & C_{52} & C_{53} & C_{54} & C_{55} & C_{56} \\ C_{61} & C_{62} & C_{63} & C_{64} & C_{65} & C_{66} \end{pmatrix} \begin{pmatrix} e_{xx} \\ e_{yy} \\ e_{zz} \\ e_{yz} \\ e_{zx} \\ e_{xy} \end{pmatrix}, \quad (3.3)$$

where σ_{ij} ($i, j = x, y, z$) are the stress components, e_{ij} ($i, j = x, y, z$) are the strain components, and $C_{\lambda\alpha}$ ($\lambda, \alpha = 1, 2, 3, \dots, 6$) are the elastic constants in the unit of GPa. In the general form, the matrix of elastic components should contain 81 components. However, due to the symmetry of σ_{ij} and e_{ij} , each of them have only 6 independent

components. Therefore, we need only 36 elastic constants as shown in Equation 3.3. These elastic constants are denoted as C_{mn} , where the indices m and n are defined as 1= xx , 2= yy , 3= zz for the compression components and 4= yz,zy ; 5= zx,xz ; 6= xy,yx for the shear components (Kittel, 1996).

The final number of independent elastic constants can be further reduced based on the level of symmetry of crystal structure. In principle, all of 36 elastic constants are independent. In practice, many of them are the same due to material symmetries. In particular, the crystal with cubic symmetry has much reduced number of independent elastic constants, i.e., $C_{11} = C_{22} = C_{33}$, $C_{12} = C_{21} = C_{23} = C_{32} = C_{13} = C_{31}$, and $C_{44} = C_{55} = C_{66}$. In addition, by symmetry, the off-diagonal shear components are also vanished, i.e., $C_{45} = C_{54} = C_{56} = C_{65} = C_{46} = C_{64} = 0$ and the mixed compression/shear couplings do not occur i.e. $C_{14} = C_{41} = \dots = 0$. Therefore, the elastic constants matrix for a cubic crystal has the form (Kittel, 1996),

$$\begin{pmatrix} C_{11} & C_{12} & C_{12} & 0 & 0 & 0 \\ C_{12} & C_{11} & C_{12} & 0 & 0 & 0 \\ C_{12} & C_{12} & C_{11} & 0 & 0 & 0 \\ 0 & 0 & 0 & C_{44} & 0 & 0 \\ 0 & 0 & 0 & 0 & C_{44} & 0 \\ 0 & 0 & 0 & 0 & 0 & C_{44} \end{pmatrix}. \quad (3.4)$$

There are only three independent elastic constants; (1) C_{11} which is based on the longitudinal compression, (2) C_{12} , which is based on the transverse expansion and (3) C_{44} , which is the shear modulus. The schematic representations of the three elastic constants of materials with the cubic symmetries are represented in Figure 3.2. To obtain elastic constants from first principles calculations there are two approaches: stress-strain methods and energy-strain method (Kittel, 1996; Elliott, 1998).

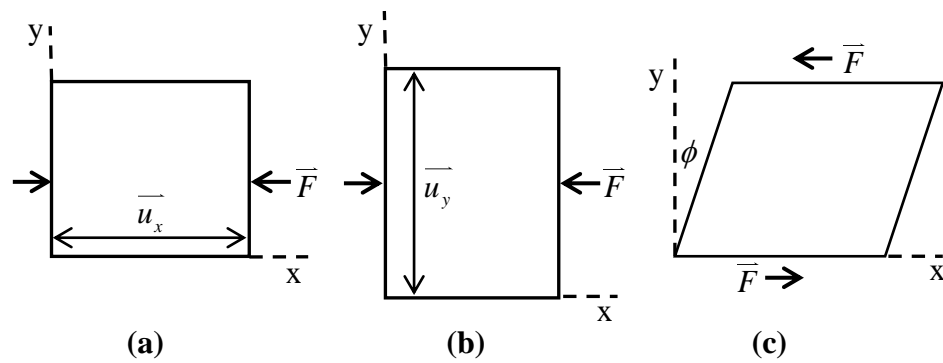


Figure 3.2 Representation of (a) longitudinal compression (C_{11}), (b) transvers expansion (C_{12}) and (c) shear modulus (C_{44}). The figure is reproduced based on the work of Elliott. (Elliott, 1998).

3.2.3 Elastic constants calculations

The elastic constants of materials with known microscopic structure can be obtained by *ab-initio* calculations using two major approaches (Le Page and Saxe, 2002). The first approach is based on the analysis of the changes in the (calculated) stress values resulting from the changes in the strain. This approach is called “stress–strain approach” (Nielsen and Martin, 1983). In practice, the stresses can be obtained from the “Hellmann-Feynman theorem”. Another approach, called “energy–strain approach” (Le Page and Saxe, 2001), is based on the analysis of the total energies of different strained states of the material.

In this work, the energy-strain approach was used to obtain the elastic constants of selected perovskite oxides. Under small deformations, the stresses can be approximated to be linearly proportional to the displacements of atoms, i.e., the potentials can be considered to be harmonic. Under this approximation, the elastic

energy density can be expressed as a quadratic function of the strains. The elastic energy density can be written as (Kittel, 1996),

$$U = \frac{1}{2} \sum_{i=1}^6 \sum_{j=1}^6 C_{ij} e_i e_j \quad (3.5)$$

where the indices 1, 2, 3, ..., 6 are defined in the same way as Equation 3.4. Each elastic constant C_{ij} can be obtained from the derivative of U with respect to the associated strain components (Kittel, 1996).

In our work, the total energy (E) is calculated for the difference predefined (small) strain ($e_{xx}, e_{yy}, e_{zz}, e_{zy}, e_{zx}, e_{xy}$) configurations. For each strain configuration, E is also calculated at a few values of the strains (e) (Wright, 1997). The energy–strain curve for each strain configuration is fitted to a third–degree polynomial function. Then, the second derivative of energy with respect to strain gives the elastic constants.

For cubic materials, the three independent of elastic constants can be obtained (among various possible sets of strain configurations) using the following set of strain configurations. The first component of elastic constants of cubic structure C_{11} can be obtained by using the strain configuration $D_1 = (e, 0, 0, 0, 0, 0)$. The elastic energy density under this strain configuration can be written in the matrix form as

$$U_1 = \frac{1}{2} (e, 0, 0, 0, 0, 0) \begin{pmatrix} C_{11} & C_{12} & C_{12} & 0 & 0 & 0 \\ C_{12} & C_{11} & C_{12} & 0 & 0 & 0 \\ C_{12} & C_{12} & C_{11} & 0 & 0 & 0 \\ 0 & 0 & 0 & C_{44} & 0 & 0 \\ 0 & 0 & 0 & 0 & C_{44} & 0 \\ 0 & 0 & 0 & 0 & 0 & C_{44} \end{pmatrix} \begin{pmatrix} e \\ 0 \\ 0 \\ 0 \\ 0 \\ 0 \end{pmatrix}. \quad (3.6)$$

The multiplication product of the matrices in the right hand side of Equation 3.6 gives

$U_1 = \frac{1}{2} C_{11} e^2$. By calculating the total energies of the material under a few values of the strain, e , the energy-strain curve can be obtained. Then the energy-strain curve is fitted to the third-degree polynomials and second derivative of the energy with respect to the strain gives C_{11} .

The second component of elastic constants, C_{12} , can be obtained by using the strain configuration $D_2 = (e, e, 0, 0, 0, 0)$, where the elastic energy density can be written in the matrix form as

$$U_2 = \frac{1}{2} (e, e, 0, 0, 0, 0) \begin{pmatrix} C_{11} & C_{12} & C_{12} & 0 & 0 & 0 \\ C_{12} & C_{11} & C_{12} & 0 & 0 & 0 \\ C_{12} & C_{12} & C_{11} & 0 & 0 & 0 \\ 0 & 0 & 0 & C_{44} & 0 & 0 \\ 0 & 0 & 0 & 0 & C_{44} & 0 \\ 0 & 0 & 0 & 0 & 0 & C_{44} \end{pmatrix} \begin{pmatrix} e \\ e \\ 0 \\ 0 \\ 0 \\ 0 \end{pmatrix}. \quad (3.7)$$

The multiplication product of the matrices in the right hand side of Equation 3.7 gives $U_2 = (C_{11} + C_{12})e^2$. The second derivative of the energy with respect to the strain gives us $2(C_{11} + C_{12})$.

The last component of elastic constants, C_{44} , can be obtained by using the strain configuration $D_3 = (0, 0, 0, e, 0, 0)$, where the elastic energy density can be written in the matrix form as

$$U_3 = \frac{1}{2} (0, 0, 0, e, 0, 0) \begin{pmatrix} C_{11} & C_{12} & C_{12} & 0 & 0 & 0 \\ C_{12} & C_{11} & C_{12} & 0 & 0 & 0 \\ C_{12} & C_{12} & C_{11} & 0 & 0 & 0 \\ 0 & 0 & 0 & C_{44} & 0 & 0 \\ 0 & 0 & 0 & 0 & C_{44} & 0 \\ 0 & 0 & 0 & 0 & 0 & C_{44} \end{pmatrix} \begin{pmatrix} 0 \\ 0 \\ 0 \\ e \\ 0 \\ 0 \end{pmatrix}. \quad (3.8)$$

The multiplication product of the matrices in the right hand side of Equation 3.8 gives

$U_3 = \frac{1}{2} C_{44} e^2$. The second derivative of the energy with respect to the strain gives us

C_{44} .

Our calculated values of the elastic constants for selected perovskite materials compared with available theoretical and experimental results are shown in Table 3.3.

Our calculated values are in reasonable agreements with available literature.

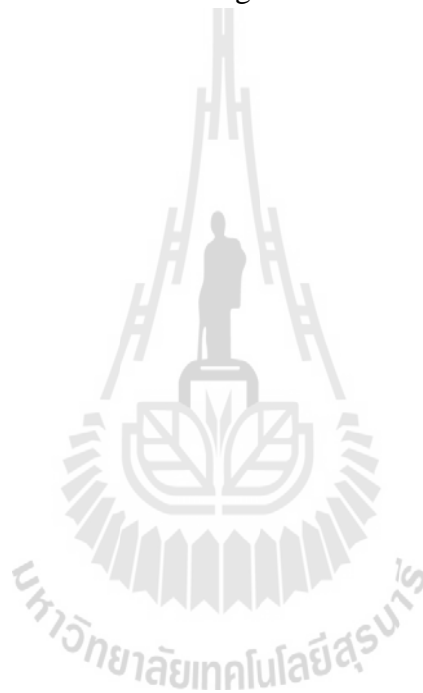


Table 3.3 Calculated elastic constants (in GPa) for selected cubic perovskite materials. Values in parentheses are from the literature.

Materials	LDA			GGA		
	C_{11}	C_{12}	C_{44}	C_{11}	C_{12}	C_{44}
BeTiO ₃	363	121	48	307	112	48
MgTiO ₃	380	110	73	339	102	72
CaTiO ₃	405	110	100	356	103	98
SrTiO ₃	385	113	119	326	103	112
	(421 ^a ,317 ^d)	(121 ^a ,102 ^d)	(133 ^a ,123 ^d)	(313 ^a ,311 ^c)	(98 ^a ,99 ^c)	(113 ^a ,104 ^c)
BaTiO ₃	357	123	137	303	111	125
	(358 ^a ,305 ^e)	(115 ^a ,106 ^e)	(150 ^a ,128 ^e)	(301 ^a)	(104 ^a)	(132 ^a)
SnTiO ₃	280	145	91	319	131	86
PbTiO ₃	328	127	102	280	116	97
	(450 ^a ,383 ^b)	(261 ^a ,151 ^b)	(113 ^a ,120 ^b)	(325 ^a)	(158 ^a)	(107 ^a)
PbZrO ₃	363	93	64	317	88	64
PbHfO ₃	379	96	76	338	93	75

^aCalculations by Piskunov *et al.* (Piskunov *et al.*, 2004)

^bCalculations by Liu *et al.* (Liu *et al.*, 2008)

^cCalculations by Boudali *et al.* (Boudali *et al.*, 2009)

^dExperimental by Bell and Rupprecht (Bell and Rupprecht, 1963)

^eCalculations by Wang *et al.* (Wang *et al.*, 2010)

3.3 Sound velocities in anisotropic materials

To model the propagation of the sound wave in anisotropic materials, we assume that atoms can be oscillated around their equilibrium positions, leading to the lattice vibrations. When considering the lattice vibrations, three major assumptions are made; (i) the displacements of the atoms from their equilibrium positions are small ($u_i \ll a$, where a is a lattice parameter), (ii) the forces acting on atoms are linearly proportional to the displacements, and (iii) adiabatic approximation is valid, i.e., the electron cloud is moved along with the atoms and the bond strength is not affected by the vibrations. In addition, the material is treated as a continuous medium not a discrete one. The vibrations are referred to as the elastic waves.

To understand the elastic wave, we first consider a segment of a long bar with the width dx . The elastic displacement of the segment dx is denoted by u as illustrated in Figure 3.3(a). Based on Newton's second law, the equation of motion can be written as

$$\sum \bar{F} = m \frac{d^2 u}{dt^2}, \quad (3.9)$$

which implies that

$$\bar{F}(x+dx) - \bar{F}(x) = (\rho A dx) \frac{d^2 u}{dt^2}, \quad (3.10)$$

where ρ is the mass density and A is the cross-section area of the bar. Eq. (3.10) can be simplified as

$$\frac{d\bar{F}}{A \cdot dx} = \rho \frac{d^2 u}{dt^2}. \quad (3.11)$$

From the definition of stress, Equation (3.11) can be written as

$$\frac{d\sigma_{xx}}{dx} = \rho \frac{d^2u}{dt^2}, \quad (3.12)$$

where σ_{xx} is the compressive stress. If the wave propagates along [100] direction, Hook's law can be written by

$$\sigma_{xx} = C_{11}e_{xx}, \quad (3.13)$$

where C_{11} is the longitudinal compression or Young's modulus and $e_{xx} = du_x/dx$ is the tensile strain. Substitute Equation (3.13) and the definition of the tensile strain into Equation (3.12), we get

$$\frac{d^2u}{dt^2} = \left(\frac{C_{11}}{\rho} \right) \frac{d^2u}{dx^2}. \quad (3.14)$$

For a longitudinal wave, the solution of the wave equation (3.14) can be written as

$$u(x,t) = Ae^{i(qx - \omega t)}, \quad (3.15)$$

where q is the wave vector and ω is the frequency which can be written as

$$\omega = v_L q. \quad (3.16)$$

v_L is the longitudinal sound velocity which can be written as a function of the elastic constants as

$$v_L = (C_{11} / \rho)^{\frac{1}{2}}. \quad (3.17)$$

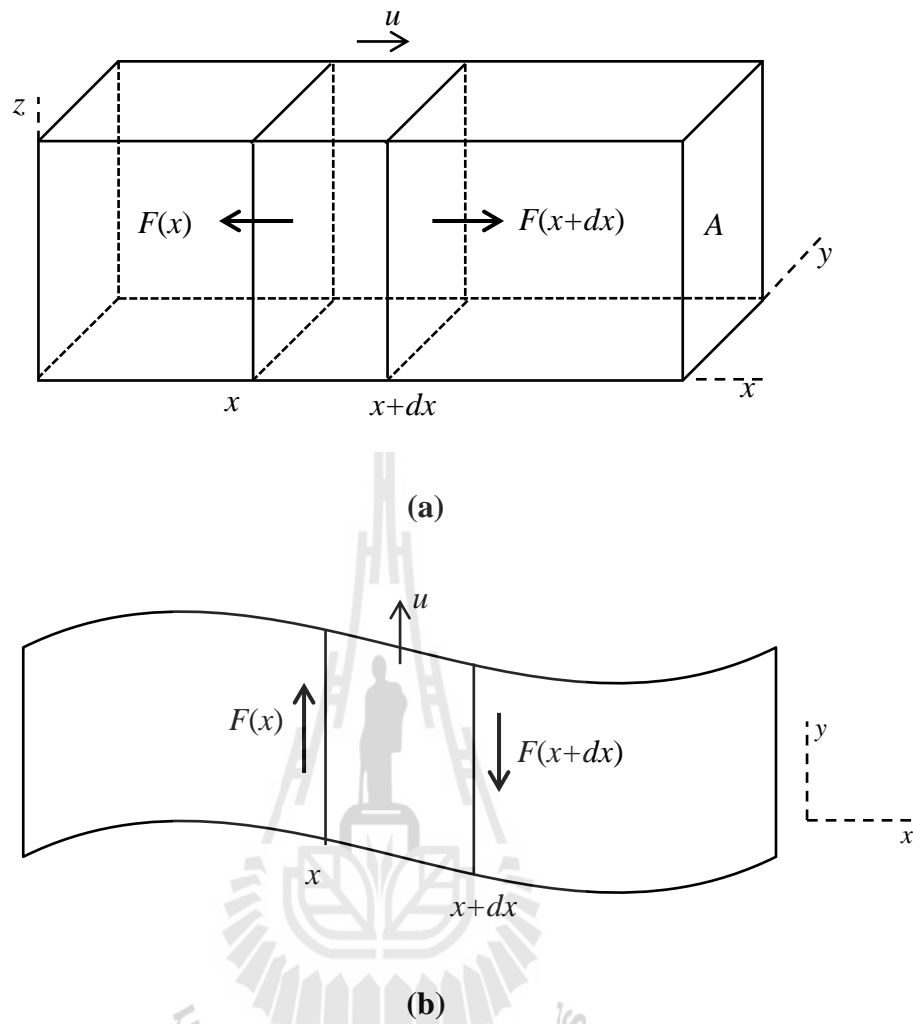


Figure 3.3 Representation of (a) the longitudinal wave and (b) the transverse wave in a slab. The figure is reproduced from Ref. (Elliott, 1998)

In the case of a transvers wave, the equation motion is based on the shear stress and strain. Consider Figure 3.3(b), in the same way as the longitudinal wave, the equation of motion for the transverse wave can be written as

$$\frac{d\sigma_{xy}}{dx} = \rho \frac{d^2u}{dt^2} \quad (3.18)$$

where σ_{xy} is the shear stress which is related to the shear modulus and shear strain by the relationship

$$\sigma_{xy} = C_{44}e_{xy} \quad (3.19)$$

$e_{xy} = du_y/dx$ is the shear strain. Substitute Equation (3.19) and the definition of shear strain into Equation (3.18), we get the transverse wave equation as

$$\frac{d^2u}{dt^2} = \left(\frac{C_{44}}{\rho} \right) \frac{d^2u}{dx^2} \quad (3.20)$$

The displacement is in the y direction when the wave propagates in the x direction. The solution of Equation (3.20) can be written as

$$u(x,t) = Ae^{i(qx-\omega t)} y, \quad (3.21)$$

where q is the wave vector and ω is the frequency, which can be written as

$$\omega = v_T q. \quad (3.22)$$

v_T is the transverse sound velocity, which can be written as a function of the elastic constants as

$$v_L = (C_{44} / \rho)^{\frac{1}{2}}. \quad (3.23)$$

Note that there are two linear independent transverse modes characterized by the displacement in y and z directions. For [100] direction, the velocities of these modes are the same due to the symmetry. Normally, C_{11} is larger than C_{44} , therefore, the

longitudinal sound velocities are generally larger than the transverse sound velocities. The sound velocities mentioned above are in [100] direction. For other directions, the sound velocities depend on the combinations of the elastic constants. The detailed derivations can be found in Ref. (Kittel, 1996). The relationships of the sound velocities and the elastic constants for a cubic crystal are summarized in Table 3.4. The schematic illustration of the propagation directions of elastic waves and the directions of the sound velocities are illustrated in Figure 3.4

Table 3.4 Sound velocity expressions of each wave propagation direction for a cubic crystal (Kittel, 1996).

Sound velocity in different directions	Expression
$v_L([100])$	$(C_{11}/\rho)^{1/2}$
$v_T([100])$	$(C_{44}/\rho)^{1/2}$
$v_L([110])$	$[(C_{11} + C_{12} + 2C_{44})/2\rho]^{1/2}$
$v_T([110])$	$[(C_{11} - C_{12})/2\rho]^{1/2}$
$v_L([111])$	$[(C_{11} + 2C_{12} + 4C_{44})/3\rho]^{1/2}$
$v_T([111])$	$[(C_{11} - C_{12} + C_{44})/3\rho]^{1/2}$

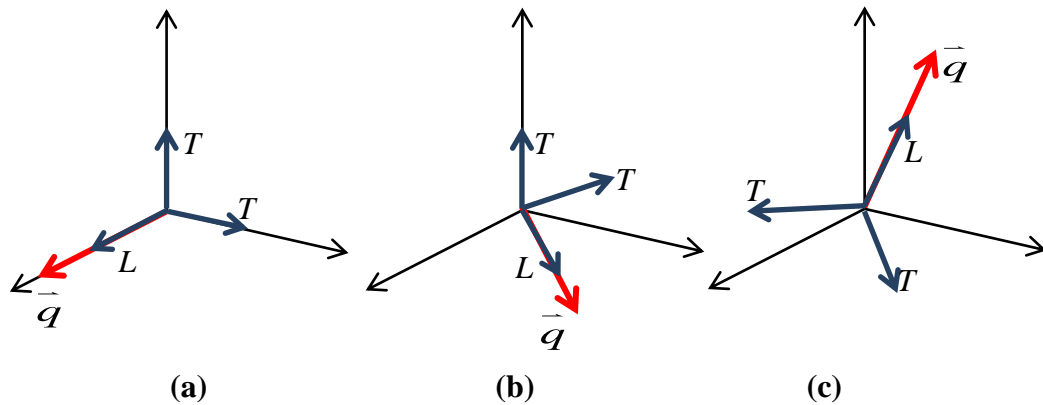


Figure 3.4 Representation of an elastic wave in a cubic crystal for (a) wave propagating in the [100] direction, (b) the [110] direction and (c) the [111] direction. Two transverse modes are degenerate for the propagation in the [100] and the [111] directions. The red arrows represent the direction of wave vector and the dark blue arrows represent the direction of the oscillation. The figure is reproduced from Ref. (Kittel, 1996)

3.4 References

- Ali, R. and Yashima, M. (2005). Space group and crystal structure of the Perovskite CaTiO_3 from 296 to 1720 K. **Journal of Solid State Chemistry** 178: 2867.
- Avinash Daga, Smita Sharma and K. S. Sharma (2011). First principle study of Cubic SrMO_3 Perovskites (M = Ti, Zr, Mo, Rh, Ru). **Journal of Modern Physics** 02: 812.
- Baedi, J., Hosseini, S. M., Kompany, A. and Kakhki, E. A. (2008). Structural, electronic and optical properties of lead zirconate. **Physica Status Solidi (b)** 245: 2572.
- Bell, R. O. and Rupprecht, G. (1963). Elastic constants of strontium titanate. **Physical Review** 129: 90.
- Boudali, A., Khodja, M. D., Amrani, B., Bourbie, D., Amara, K. and Abada, A. (2009). First-principles study of structural, elastic, electronic, and thermal properties of SrTiO_3 perovskite cubic. **Physics Letters A** 373: 879.
- Brendan, J. K., Christopher, J. H. and Bryan, C. C. (1999). Phase transitions in perovskite at elevated temperatures - a powder neutron diffraction study. **Journal of Physics: Condensed Matter** 11: 1479.
- Howard C. J., Kennedy B. J. and Woodward P. M. (2003). Ordered double perovskites - a group-theoretical analysis. **Acta Crystallogr B** 59: 463.
- Elliott, S. (1998). **The Physics and Chemistry of Solids**. Chichester, England: John Wiley & Sons.
- Fujishita, H., Ishikawa, Y., Tanaka, S., Ogawaguchi, A. and Katano, S. (2002). Crystal structure and order parameters in the phase transition of antiferroelectric PbZrO_3 . **Journal of the Physical Society of Japan** 72: 1426.

- Howard, C. J. and Stokes, H. T. (2002). Group-theoretical analysis of octahedral tilting in perovskites. Erratum. **Acta Crystallographica Section B** 58: 565.
- Johnsson, M. and Lemmens, P. (2007) Crystallography and Chemistry of Perovskites. In Handbook of Magnetism and Advanced Magnetic Materials John Wiley & Sons, Ltd.
- K.H. Hellwege and A.M. Hellwege (1969). Ferroelectrics and Related Substances. **New Series, Landolt-Bornstein, Springer Verlag, Berlin, 3.**
- Kittel, C. (1996). **Introduction to Solid State Physics.** United State of America: Cambridge University. John Wiley & Sons, Inc.
- Le Page, Y. and Saxe, P. (2001). Symmetry-general least-squares extraction of elastic coefficients from *ab initio* total energy calculations. **Physical Review B** 63: 174103.
- Le Page, Y. and Saxe, P. (2002). Symmetry-general least-squares extraction of elastic data for strained materials from *ab initio* calculations of stress. **Physical Review B** 65: 104104.
- Lee, H., Mizoguchi, T., Yamamoto, T. and Ikuhara, Y. (2009). First principles study on intrinsic vacancies in cubic and orthorhombic CaTiO₃. **Materials Transactions** 50: 977.
- Liu, Y., Xu, G., Song, C., Ren, Z., Han, G. and Zheng, Y. (2008). First-principles study of elastic properties in perovskite PbTiO₃. **Materials Science and Engineering: A** 472: 269.
- Megaw, H. D. (1973). Crystal Structure - A Working Approach. **Philadelphia: W. B. Saunders.**
- Mitchell, R. H. (2002). Perovskites: Modern and Ancient **Ontario: Almaz Press Inc.**

- Nielsen, O. H. and Martin, R. M. (1983). First-principles calculation of stress. **Physical Review Letters** 50: 697.
- Pandech, N., Sarasamak, K. and Limpijumnong, S. Sound velocities and elastic properties of PbTiO_3 and PbZrO_3 under pressure: First principles study. **Ceramics International**. 39: S277.
- Parker, W. D., Rondinelli, J. M. and Nakhmanson, S. M. (2011). First-principles study of misfit strain-stabilized ferroelectric SnTiO_3 . **Physical Review B** 84: 245126.
- Piskunov, S., Heifets, E., Eglitis, R. I. and Borstel, G. (2004). Bulk properties and electronic structure of SrTiO_3 , BaTiO_3 , PbTiO_3 perovskites: an *ab initio* HF/DFT study. **Computational Materials Science** 29: 165.
- Shirane, G., Pepinsky, R. and Frazer, B. C. (1956). X-ray and neutron diffraction study of ferroelectric PbTiO_2 . **Acta Crystallographica** 9: 131.
- Wang, J. J., Meng, F. Y., Ma, X. Q., Xu, M. X. and Chen, L. Q. (2010). Lattice, elastic, polarization, and electrostrictive properties of BaTiO_3 from first-principles. **Journal of Applied Physics** 108: 034107.
- Wang, Y. X., Arai, M., Sasaki, T., Wang, C. L. and Zhong, W. L. (2005). First-principles study on the (0,0,1) surface of cubic PbZrO_3 and PbTiO_3 . **Surface Science** 585: 75.
- Wright, A. F. (1997). Elastic properties of zinc-blende and wurtzite AlN , GaN , and InN . **Journal of Applied Physics** 82: 2833.

CHAPTER IV

SOUND VELOCITIES AND ELASTIC PROPERTIES OF PbTiO₃ AND PbZrO₃ UNDER PRESSURE: FIRST PRINCIPLES STUDY

4.1 Introduction

PbZrO₃ (PZO) and PbTiO₃ (PTO) are the parent compound materials of the extensively utilized ferroelectric material Pb(Ti,Zr)O₃ (PZT). PZT (as well as PZO and PTO) has perovskite structure and is used in many devices such as ultrasonic transducers and piezoelectric actuators (Yamamoto and Makino, 1996). The room temperature phase of PZO and PTO is orthorhombic and tetragonal structure, respectively (Kagimura and Singh, 2008; Kalinichev *et al.*, 1997). Both orthorhombic PZO and tetragonal PTO have only slight distortion from the perfect cubic perovskite structure. The elastic properties of PZO and PTO under ambient pressure have been studied by various research groups. Liu and co-workers (Liu *et al.*, 2008) theoretically studied the elastic properties of PTO in both cubic and tetragonal phases. Kalinichev and co-workers (Kalinichev *et al.*, 1997) used brillouin light scattering on single crystalline PTO samples to obtain the elastic and piezoelectric constants at room temperature. For PZO, Kagimura and D. J. Singh (Kagimura and Singh, 2008) studied the elastic properties and energetics of orthorhombic and rhombohedral phases.

The effects of hydrostatic pressure on perovskite materials have been experimentally and theoretically investigated. However, to our knowledge, the elastic properties and sound velocities of PTO and PZO under pressure have not been reported. For PTO, most of previous works were performed in order to understand their ferroelectric properties under pressure. Liu and co-workers (Liu *et al.*, 2008) focused mainly on the calculations of equilibrium tetragonal to cubic phase transition pressure of PTO.

In this chapter, the elastic constants and sound velocities of cubic perovskite PZO and PTO under pressures were studied based on density functional theory calculations.

4.2 Computational Method

The computational approach employed was based on first principles density functional theory (Hohenberg and Kohn, 1964; Kohn and Sham, 1965) with plane wave pseudo-potentials as implemented in the Vienna *Ab-initio* Simulation Package (VASP) code (Kresse and Furthmüller, 1996). For the exchange correlation terms, both local density approximation (LDA) (Ceperley and Alder, 1980; Perdew and Zunger, 1981) and generalized gradient approximation (GGA) (Perdew *et al.*, 1997) were used. The ultrasoft version of the pseudo-potential implemented in the VASP code allows a low cut off energies for the plane wave expansion (only 500 eV). We used a $8 \times 8 \times 8$ Monkhorst-Pack scheme (Monkhorst and Pack, 1976) *k*-point sampling.

In our calculations, the structures of PTO and PZO were treated as ideal cubic structures with the space group $Pm\bar{3}m$ (#221) as illustrated in Figure. 3.1. The atomistic positions follow the Wychoff positions: Pb 1a (0,0,0), Ti (or Zr) 1b (0.5,0.5,0.5) and O 3c (0,0.5,0.5), (0.5,0.5,0) and (0.5,0.0.5) as shown in Table 3.1.

To study the elastic properties, the total energies (E) of a unit cell of material at several slightly different volumes (V) were calculated and fitted into an equation of states (Li *et al.*, 2005). If the unit cell is uniformly scaled, to simulate the hydrostatic pressure effect, the bulk modulus (B_0) and its pressure derivative (B') is obtained. Under the same approach, other elastic constants and sound velocities can be calculated as described in Sarasamak *et al.* (Sarasamak *et al.*, 2010). The reduced material volume can be translated into the corresponding pressure following the pressure–volume (P – V) relationship constructed by Birch-Murnaghan's equation of state (Poirier, 2000) written as,

$$P(V) = \frac{3B_0}{2} \left[\left(\frac{V_0}{V} \right)^{7/3} - \left(\frac{V_0}{V} \right)^{5/3} \right] \left\{ 1 + \frac{3}{4} (B' - 4) \left[\left(\frac{V_0}{V} \right)^{2/3} - 1 \right] \right\}, \quad (4.1)$$

where V_0 is the equilibrium volume.

4.3 Results and Discussion

4.3.1 Structural and elastic properties

The calculated equilibrium lattice constants as well as the corresponding volumes of both PTO and PZO calculated based on both LDA and GGA exchange correlation functional are shown in Table 4.1 in comparison with other computation and experimental results. Our values are in agreement with other corresponding calculated results. In comparison with the experimental value, LDA tends to give a slightly smaller lattice constant while GGA tends to give a larger value. This is consistent with what have generally been observed in other materials.

The calculated bulk modulus (B), its pressure derivative (B'), and the elastic constants at zero pressure of both PTO and PZO are also shown in Table 4.1. Because LDA gives a smaller lattice constant compared to the corresponding value obtained using GGA, the bulk moduli and all elastic constants computed using LDA are consistently higher than the corresponding ones computed using GGA. PTO has been previously studied by Piskunov *et al.* (Piskunov *et al.*, 2004) and Liu *et al.* (Liu *et al.*, 2008). Liu's LDA results are consistently higher than our results while their GGA results are quite similar. To our knowledge, there is no computation result available for PZO. The sound velocities, shown in the bottom section of Table 4.1, can be derived from the elastic constants using the expressions shown in Table 3.4.

Table 4.1 Calculated lattice constants (a) in Å, a unit cell volumes (V_0) in Å³, bulk modulus (B) in GPa, its pressure derivative (B'), elastic constants in GPa and sound velocities in km/s of PbTiO₃ and PbZrO₃ in the cubic perovskite structure compared with the literature.

		PbTiO ₃		PbZrO ₃	
		LDA	GGA	LDA	GGA
a	Present	3.89	3.97	4.13	4.20
	Other Calc.	3.88 ^a , 3.93 ^b	3.98 ^a , 3.96 ^b	4.11 ^c	4.19 ^c , 4.18 ^d
	Expt.	3.95 ^e		4.16 ^f	
V_0	Present	58.76	63.32	70.22	74.08
B	Present	219	185	181	168
	Other Calc.	229 ^g , 324 ^b	213 ^b	-	-
B'	Present	4.5	3.5	4.6	3.7
C_{11}	Present	380	316	366	322
	Other Calc.	384 ^g , 450 ^b	325 ^b	-	-
C_{12}	Present	145	130	92	89
	Other Calc.	151 ^g , 261 ^b	158 ^b	-	-
C_{44}	Present	103	96	63	62
	Other Calc.	120 ^g , 113 ^b	107 ^b	-	-
$v_L[100]$	Present	6.66	6.25	6.69	6.42
$v_T[100]$	Present	3.46	3.44	2.78	2.82
$v_L[110]$	Present	6.53	6.28	5.98	5.86
$v_T[110]$	Present	3.70	3.39	4.10	3.86
$v_L[111]$	Present	6.48	6.43	5.72	5.65
$v_T[111]$	Present	3.63	3.55	3.71	3.55

^a Calculations by Hosseini *et al.* (Hosseini *et al.*, 2007)

^b Calculations by Piskunov *et al.* (Piskunov *et al.*, 2004)

^c Calculations by Wang *et al.* (Wang *et al.*, 2005)

^d Calculations by Baedi *et al.* (Baedi *et al.*, 2008)

^e Measurements by Kuroiwa *et al.* (Kuroiwa *et al.*, 2001)

^f Measurements by Fujiishita *et al.* (Fujiishita *et al.*, 2002)

^g Calculations by Liu *et al.* (Liu *et al.*, 2008)

4.3.2 Elastic properties under pressure

To study the elastic constants and sound velocities under hydrostatic pressures, the calculations were performed at several reduced volumes, each of which corresponds to the system under a different pressure. The pressure can be determined from the pressure-volume relation shown by Equation 4.1. Sound velocities of PTO and PZO under pressure can be obtained from the corresponding elastic constants using the expressions (cite) given in Table 3.4.

The elastic constant as a function of pressure for cubic perovskite PTO and PZO are shown in Figure 4.1. The elastic constants of both materials have similar behaviors under pressure. In general, we can see that all three elastic constants, C_{11} , C_{12} and C_{44} increase with the pressure. In both PTO and PZO, C_{11} , which is related to the longitudinal distortion, rapidly increases with the pressure. On the other hand, C_{12} and C_{44} are much less sensitive to the pressure. Indeed, C_{44} , which is related to the transverse distortion, remains almost constant throughout the pressure range studied. The calculated sound velocities under pressure for both cubic perovskite PTO and PZO are shown in Figure 4.2. Since the sound velocities are directly derived from the elastic constants, similar trends were found. All of the sound velocities, except for the $v_T([100])$ of PZO, increase with pressure mainly because they contain C_{11} which rapidly increases with pressure. In PZO, $v_T([100])$ slightly decreases under pressure because it associated only with C_{44} which remains almost flat with pressure and divided by ρ which increases with the pressure. As expected, the longitudinal modes are larger than the transverse modes such that they can be divided into two groups.

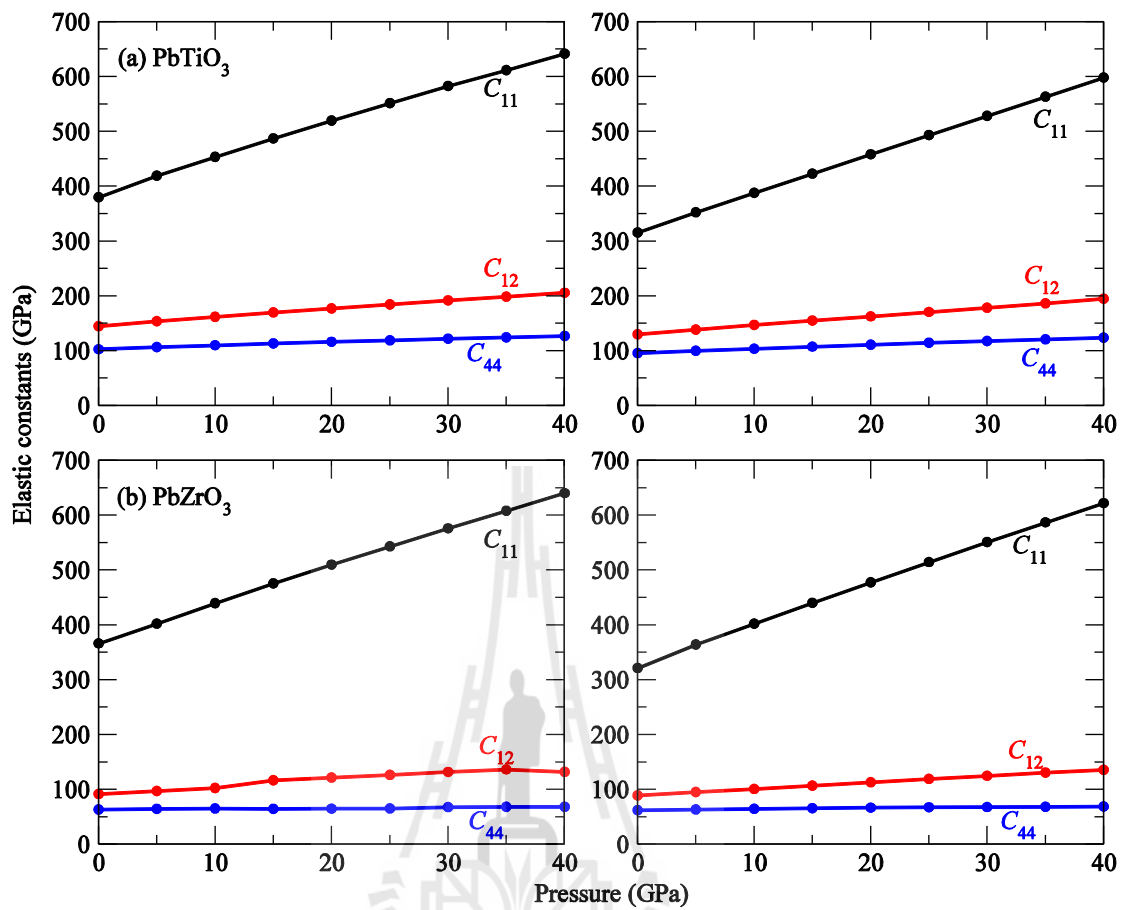


Figure 4.1 Elastic constants as a function of pressure for cubic perovskite PbTiO_3 and PbZrO_3 , obtained from LDA (left) and GGA (right).

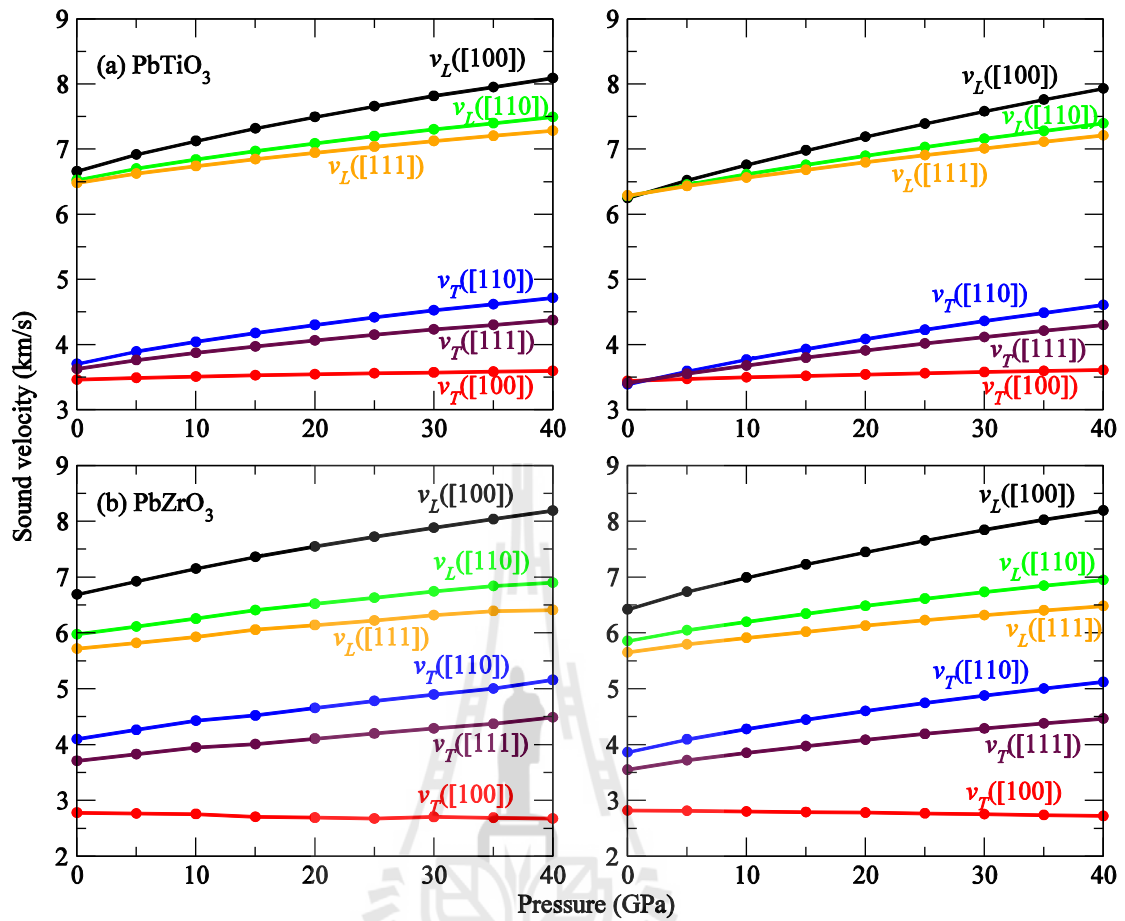


Figure 4.2 Sound velocities as a function of pressure for cubic perovskite PbTiO_3 and PbZrO_3 , obtained from LDA (left) and GGA (right).

4.4 Conclusions

The elastic constants and sound velocities of cubic perovskite PTO and PZO as a function of pressure were calculated by first principles calculations. Both LDA and GGA exchange and correlations were used. The calculated zero-pressure properties are in good agreement with literature; ensuring the validity of the results. LDA gives slightly smaller lattice constants and larger bulk moduli than GGA which is consistent with what have been observed in other materials. The elastic constants and sound velocities under the pressure range of 0–40 GPa were presented. The elastic constants almost linearly increased with pressure. C_{11} rapidly increases with pressure while C_{12} and C_{44} are much less sensitive to pressure. Because the sound velocities are related to the elastic constants, almost all of them increase with pressure.

4.5 References

- Baedi, J., Hosseini, S. M., Kompany, A. and Kakhki, E. A. (2008). Structural, electronics and optical properties of lead zirconate. **Physica status solidi (b)** 245: 2572.
- Ceperley, D. M. and Alder, B. J. (1980). Ground state of the electron gas by a stochastic method. **Physical Review Letters** 45: 566.
- Fujishita, H., Ishikawa, Y., Tanaka, S., Ogawaguchi, A. and Katano, S. (2002). Crystal structure and order parameters in the phase transition of antiferroelectric PbZrO_3 . **Journal of the Physical Society of Japan**. 72: 1426.

- Hohenberg, P. and Kohn, W. (1964). Inhomogeneous electron gas. **Physical Review** 136: B864.
- Hosseini, S. M., Movlaroooy, T. and Kompany, A. (2007). First-principle calculations of the cohesive energy and the electronic properties of PbTiO_3 . **Physica B: Condensed Matter** 391: 316.
- Kagimura, R. and Singh, D. J. (2008). First-principles investigations of elastic properties and energetics of antiferroelectric and ferroelectric phases of PbZrO_3 . **Physical Review B** 77: 104113.
- Kalinichev, A. G., Bass, J. D., Sun, B. N. and Payne, D. A. (1997). Elastic properties of tetragonal PbTiO_3 single crystals by Brillouin scattering. **Journal of Materials Research** 12: 2623.
- Kohn, W. and Sham, L. J. (1965). Self-Consistent equations including exchange and correlation effects. **Physical Review** 140: A1133.
- Kresse, G. and Furthmüller, J. (1996). Efficient iterative schemes for *ab initio* total-energy calculations using a plane-wave basis set. **Physical Review B** 54: 11169.
- Kuroiwa, Y., Aoyagi, S., Sawada, A., Harada, J., Nishibori, E., Takata, M. and Sakata, M. (2001). Evidence for Pb-O covalency in tetragonal PbTiO_3 . **Physical Review Letters**: 217601.
- Li, J. H., Liang, S. H., Guo, H. B. and Liu, B. X. (2005). Four-parameter equation of state of solids. **Applied Physics Letters**: 194111.
- Liu, Y., Xu, G., Song, C., Ren, Z., Han, G. and Zheng, Y. (2008). First-principles study of elastic properties in perovskite PbTiO_3 . **Materials Science and Engineering: A** 472: 269.

- Monkhorst, H. J. and Pack, J. D. (1976). Special points for Brillouin-zone integrations. **Physical Review B** 13: 5188.
- Perdew, J. P., Burke, K. and Ernzerhof, M. (1997). Generalized gradient approximation made simple [Phys. Rev. Lett. 77, 3865 (1996)]. **Physical Review Letters** 78: 1396.
- Perdew, J. P. and Zunger, A. (1981). Self-interaction correction to density-functional approximations for many-electron systems. **Physical Review B** 23: 5048.
- Piskunov, S., Heifets, E., Eglitis, R. I. and Borstel, G. (2004). Bulk properties and electronic structure of SrTiO₃, BaTiO₃, PbTiO₃ perovskites: an *ab initio* HF/DFT study. **Computational Materials Science** 29: 165.
- Poirier, J. P. (2000). Introduction to the Physics of the Earth Interior, second ed., Cambridge University Press, Cambridge.
- Sarasamak, K., Limpijumng, S. and Lambrecht, W. R. L. (2010). Pressure-dependent elastic constants and sound velocities of wurtzite SiC, GaN, InN, ZnO, and CdSe, and their relation to the high-pressure phase transition: A first-principles study. **Physical Review B** 82: 035201.
- Wang, Y. X., Arai, M., Sasaki, T., Wang, C. L. and Zhong, W. L. (2005). First-principles study on the (0 0 1) surface of cubic PbZrO₃ and PbTiO₃. **Surface Science** 585: 75.
- Yamamoto, T. and Makino, Y. (1996). Pressure dependence of ferroelectric properties in PbZrO₃ - PbTiO₃ solid state system under hydrostatic stress. **Japanese Journal of Applied Physics** 35: 3214

CHAPTER V

ELASTIC PROPERTIES OF PEROVSKITE $ATiO_3$

(A=Be, Mg, Ca, Sr and Ba) and $PbBO_3$ (B=Ti, Zr, and Hf)

5.1 Introduction

The elastic properties are the fundamental properties that providing detailed information on the mechanical properties of materials. Because the elastic properties can be used to describe and predict the mechanical behavior of materials in different situations, they are widely studied. For perovskite family of oxides (ABO_3), the elastic properties of several materials have been studied theoretically (computation) and experimentally.

Examples of materials that have been studied theoretically by first principles DFT calculations are $BaTiO_3$ (Meng *et al.*, 2010; Wang *et al.*, 2010), $PbTiO_3$ (Liu *et al.*, 2008), $SrTiO_3$ (Boudali *et al.*, 2009) and $SnTiO_3$ (M.F.M. Taib *et al.*, 2012).

On the experimental side, several perovskite oxides have also been studied. Li and co-workers (Li *et al.*, 1991) used the Brillouin scattering and ultrasound techniques to measure the velocity of the ultrasound in a single tetragonal $BaTiO_3$ crystal. The sound velocities can be used to calculate the elastic and piezoelectric constants. $SrTiO_3$ has also been studied different techniques (Lheureux *et al.*, 1999; Poindexter and Giardini, 1958; Schranz *et al.*, 1999). This is because $SrTiO_3$ has

rather simple structure (cubic phase at room temperature) with high quality crystal available. Lheureux and co-worker used the ultrasonic measurement technique to study the elastic constants and their pressure dependence of cubic SrTiO₃.

Although the elastic properties of some ABO_3 perovskite materials have been studied, the trend of how the elastic constants changed with the cation species has not been investigated. In this chapter, how the elastic constants change with cation species will be investigated by systematically varying A-site and B-site cations. In this work, while we vary the A-site among different Group II elements, we fix the B-site to be Ti. The A-site was fixed to be Pb when we vary the B-site among different Group IV transition elements. The cation elements used are highlighted in Figure 5.1

5.2 Computational Method

In this work, the computational approach employed is based on first principles density functional theory (DFT) (Hohenberg and Kohn, 1964; Kohn and Sham, 1965) with the plane wave pseudo-potential as implemented in Vienna *Ab-initio* Simulation Package (VASP) code (Kresse and Furthmüller, 1996). Both local density approximation (LDA) (Ceperley and Alder, 1980; Perdew and Zunger, 1981) and generalized gradient approximation (GGA) (Perdew *et al.*, 1996) were used as the exchange correlation terms. The ultrasoft version of the pseudo-potential implemented in the VASP code allows a low cut off energies for the plane wave expansion of only 500 eV. We used a 8×8×8 Monkhorst-Pack scheme (Monkhorst and Pack, 1976) k -point sampling. More detailed information on the computation approach can be found in Chapter II

In our study, the structure of selected perovskite materials was assumed to be the ideal cubic structure (space group $Pm\bar{3}m$) as illustrated in Figure 3.1 (Chapter III) with the atomistic positions following the Wychoff positions tabulated in Table 3.1. The energy-strain relation was used to determine the elastic constants. The elastic energy density (U) can be expressed as the quadratic function of the strains as, (Kittel, 1996)

$$U = \frac{1}{2} \sum_{i=1}^6 \sum_{j=1}^2 C_{ij} e_i e_j , \quad (5.1)$$

where the elastic constants C_{ij} can be obtained from the derivative of U with respect to the associated strain components (Kittel, 1996). For example, in order to calculate the C_{11} elastic constants, the strain configuration $D_1 = (e, 0, 0, 0, 0, 0)$ was used. The elastic energy density can be written in a matrix as,

$$U_1 = \frac{1}{2} (e, 0, 0, 0, 0, 0) \begin{pmatrix} C_{11} & C_{12} & C_{12} & 0 & 0 & 0 \\ C_{12} & C_{11} & C_{12} & 0 & 0 & 0 \\ C_{12} & C_{12} & C_{11} & 0 & 0 & 0 \\ 0 & 0 & 0 & C_{44} & 0 & 0 \\ 0 & 0 & 0 & 0 & C_{44} & 0 \\ 0 & 0 & 0 & 0 & 0 & C_{44} \end{pmatrix} \begin{pmatrix} e \\ 0 \\ 0 \\ 0 \\ 0 \\ 0 \end{pmatrix}. \quad (5.2)$$

The multiplication product of Equation (5.2) gives the energy of this strain configuration as $U_1 = \frac{1}{2} C_{11} e^2$. The elastic energy was calculated with the several values of the strain (e) and then the energy–strain curve was fitted to the third–degree polynomials as shown in Figure 5.2. The second derivative of the energy with respect to the strain gives us C_{11} . Other elastic components can be obtained using similar steps. More details can be found in Chapter III (Section 3.2.3).

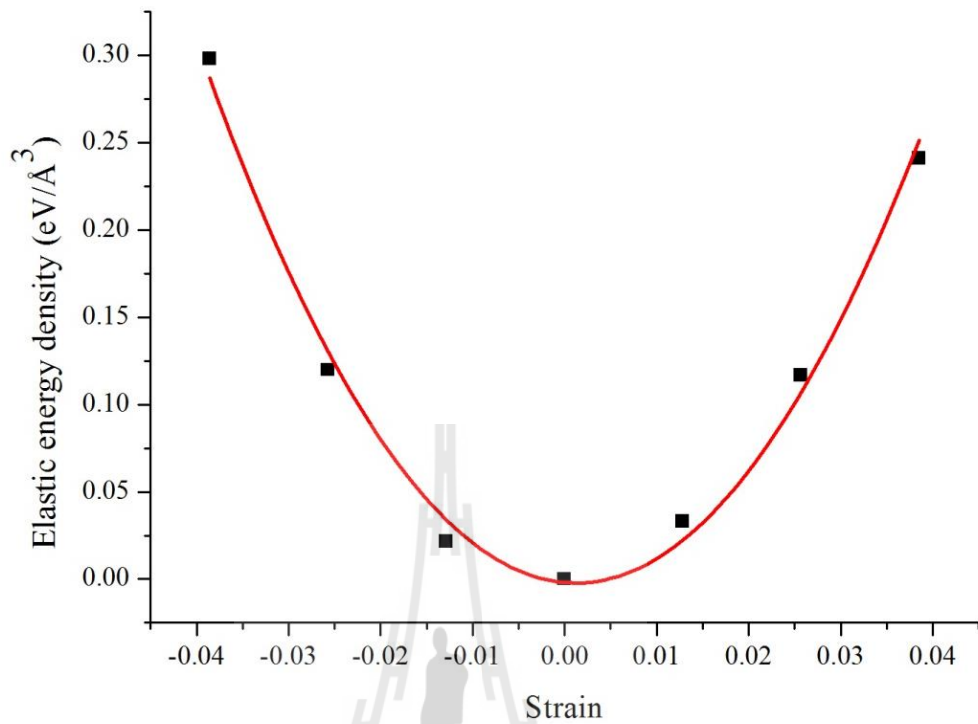


Figure 5.2 A typical energy-strain curve fitting used to obtain the elastic constants. The black square points represent the calculated data and the red curve represents the third-degree polynomial fitting.

5.3 Results and Discussion

As described in Chapter III, there are only three independent elastic constants (C_{11} , C_{12} and C_{44}) for cubic crystal. Each of them represents the directional mechanical responses of the crystal for different directions of applied forces with the details described in Chapter III (Figure 3.2 and Section 3.2). The calculated elastic constants of selected perovskite materials (according to what previously described criteria) based on both LDA and GGA exchange correlation functional are tabulated in Table 3.3. In general, LDA tends to consistently give slightly larger elastic constants than GGA. Our values are in good agreement with available calculated and experimental results.

To understand the trend of the elastic constants with respect to cation species, the elastic constants for materials with different A-site cations and B-site cations are plotted with respect to the atomic numbers of the varied cations in Figure 5.4(a)(c)(e) and (b)(d)(f), respectively.

The longitudinal elastic constant, C_{11} , directly represent the stiffness of the crystal. It is based on the longitudinal compression as shown in Figure 3.2. From the plot (Figure 5.4(a)), we can see that as we varied the A-site cation from Be to Ba, C_{11} increases until it reaches the maximum, when Ca is the A-site cation, then decreases. As we varied the B-site cation (Figure 5.4(b)), from Ti to Hf, C_{11} monotonically increases. Although the behavior of C_{11} with respect to A-site and B-site cations seems to be complicated and no clear trend, it can be explained using a simple explanation as following. The perovskite structure can be considered to be a network of two intercalating cage structures; A-site cage and oxygen cage as illustrated in Figure 5.3. Because the two networks share the same set of oxygen atoms, the

volumes of the two types of cages are not independent but tied to each other. The volumes of the two cage types are not necessarily optimized at the same time. Therefore, the overall lattice constant of the crystal is optimized at the interplay point that compromises the volumes of the two types of cages. Both networks of cages contributed into the strength (C_{11}) of the crystal. When the atomic species that occupies an A-site is smaller than that occupies a B-site, the strength of the crystal is dominated by the network of the oxygen cages. On the other hand, when the atomic species that occupies an A-site is larger than that occupies a B-site, the strength of the crystal is dominated by the network of A-site cages. The crystal becomes the most stiff (C_{11} reaches maximum) when the size of atomic species that occupies an A-site is comparable to that occupies a B-site; the point where both types of cages contributed to the stiffness of the crystal. As we varied the A-site cation and fixed the B-site cation to be Ti, the maximum C_{11} takes place when an A-site atom is Ca which has the size most comparable to Ti among all Group-II elements used. At other point, only one type of the cages is dominating the stiffness, resulting in a lower C_{11} . By using the same reasoning, the behavior of C_{11} with respect to the changes of the B-site cation, can also be explained. When we change the B-site cation, the A-site cation is fixed to be Pb. We would expect C_{11} to be the largest when the B-site cation is comparable to Pb; in this case Hf. Therefore, it is not surprising that C_{11} monotonically increases as we varied the B-site cation from Ti to Hf. C_{11} is expected to shift lower for PbRfO_3 (not calculated).

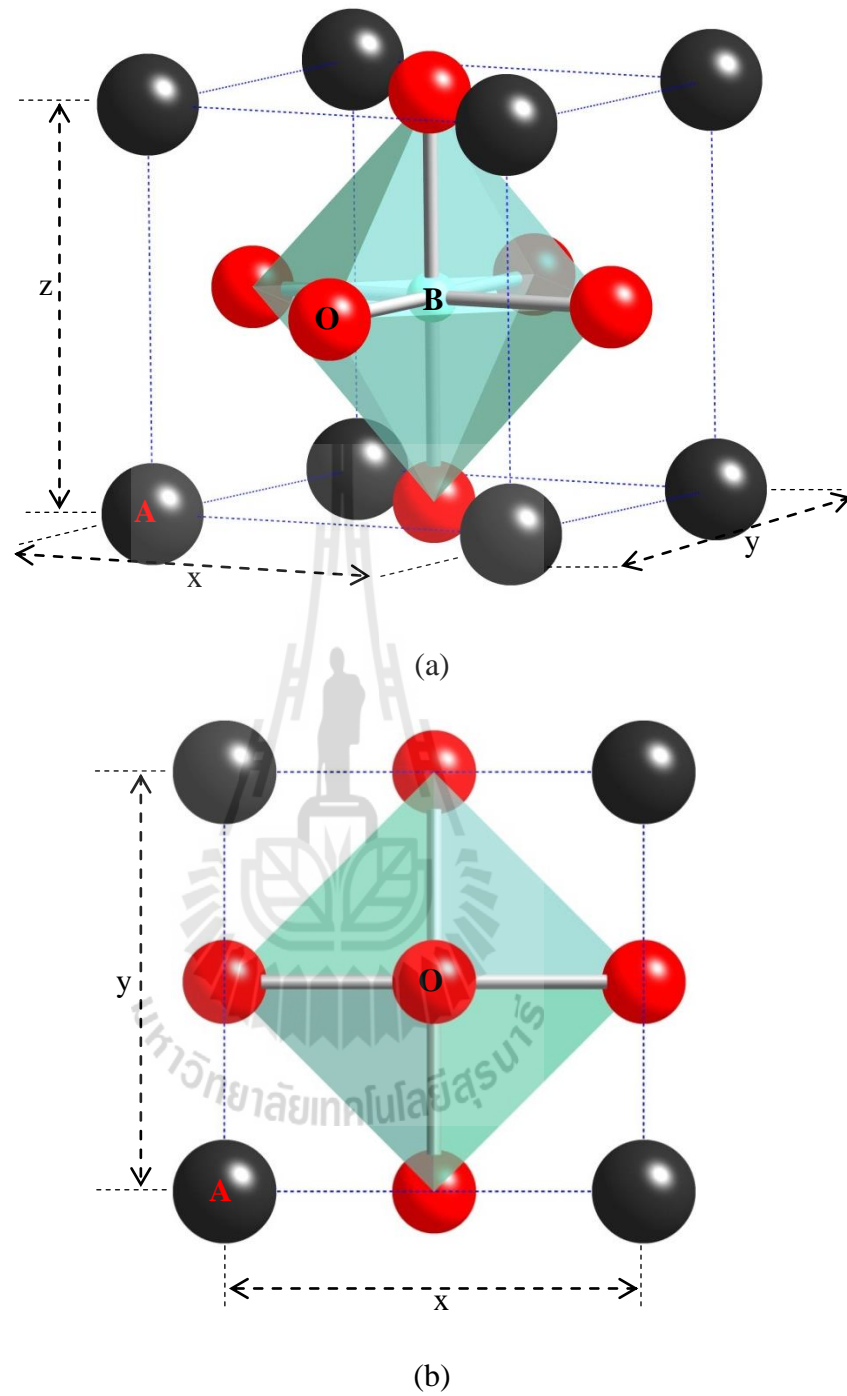


Figure 5.3 Illustration of the polyhedra of ideal cubic perovskite crystal from (a) a perspective view and (b) top view. The blue-green cage represents the oxygen cage. The dark gray spheres represent A cations, blue-green spheres are B cation, and red spheres are oxygen anions.

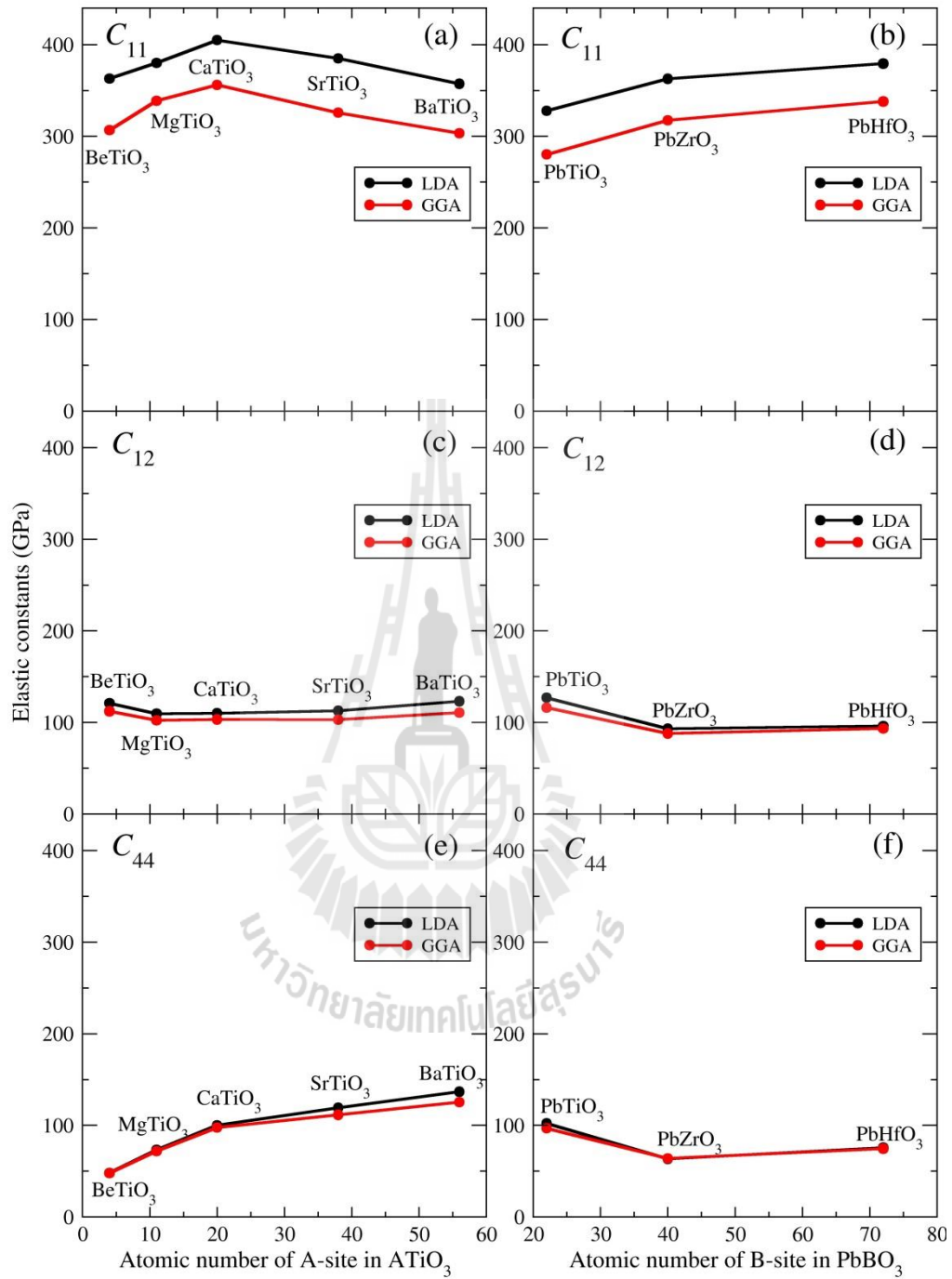


Figure 5.4 Elastic constants (C_{ij}) of perovskite (a) $ATiO_3$ and (b) $PbBO_3$ as a function of atomic number of A-site and B-site atom, respectively.

The transvers elastic constant, C_{12} , is based on the transverse expansion as shown in Figure 3.2. From the plots (Figure 5.4(c)), we can see that C_{12} is not very sensitive to the changing of A-site cations, when the B-site cation is kept fixed as Ti. This is because C_{12} is mainly dominated by the distortion of the oxygen cage, i.e., as the cage is squeezed on the side it would heavily expand in the transverse direction. As we change A-site cations, the center of the oxygen cages remains to be Ti. As a result, C_{12} remains almost constant. On the other hand, from the plot in Figure 5.4(d), C_{12} is slightly decreased as the B-site cation was changed from Ti to Zr and remained unchanged as it is changed further to a larger Hf cation. Changing B-site cations, directly affect the oxygen cages. As the B-site cations (Ti) were replaced by larger cations (Zr or Hf) the cages are expanded and the conformation of the polyhedral shape turns weaker; leading to a smaller C_{12} .

The shear elastic constant, C_{44} , is based on the distortion shown in Figure 3.2. From the plot in Figure 5.4(e), we can see that C_{44} is increased with the size of A-site cations. This indicates that C_{44} is directly dominated by the A-site cage. Because the overall lattice constant is partly controlled by the oxygen cage, for small A-site cations, the A-site cages are expanded; resulting in the weak bonds to O and small C_{44} . As the A-site cations turn larger to comparable or even larger than the B-site atom, their bonding to O becomes stronger making the A-site cage more difficult to shear. Hence, C_{44} increases. On the other hand, from the plot in Figure 5.4(f), C_{44} is decreased as the B-site cation was changed from Ti to Zr and remained almost unchanged as it is changed further to a larger Hf cation. This can be explained using the same reasoning, C_{44} is dominated by the A-site cage (in this case Pb). As the B-

site cations are changed from Ti to Zr the size of oxygen cages increase pushing the Pb-O bonds to a value larger than their optimum length leading to smaller C_{44} .

5.4 Conclusion

Elastic properties of perovskite $ATiO_3$ (A=Be, Mg, Ca, Sr and Ba) and $PbBO_3$ (B=Ti, Zr and Hf) were studied by first principles calculations. Both of LDA and GGA exchange and correlations were used in the calculations. The calculated elastic constants are in good agreement with available literatures. The LDA results consistently give slightly larger elastic constants than those calculated using GGA. For $ATiO_3$, C_{11} was found to increase with the atomic size of A until it reaches maximum when the atomic size of A-site and B-site atoms are comparable. As the atomic size of A further increased, was found to decrease. For $PbBO_3$, C_{11} was found to monotonically increase with the atomic size of B since B is always smaller than Pb in this study. C_{12} was found to be quite the same for the entire series of $ATiO_3$. However, for $PbBO_3$, C_{12} was found to slightly decrease as the size of B-site cations increases. C_{44} elastic constant was found to monotonically increase with the size of A-site cations for the $ATiO_3$ system and slightly decrease with the size of B-site cations for the $PbBO_3$. The discussions of the changes of the elastic constants with respect to the cation sizes were given based on the nature of the crystal structure.

5.5 References

- Boudali, A., Khodja, M. D., Amrani, B., Bourbie, D., Amara, K. and Abada, A. (2009). First-principles study of structural, elastic, electronic, and thermal properties of SrTiO₃ perovskite cubic. **Physics Letters A** 373: 879.
- Ceperley, D. M. and Alder, B. J. (1980). Ground state of the electron gas by a stochastic method. **Physical Review Letters** 45: 566.
- Hohenberg, P. and Kohn, W. (1964). Inhomogeneous electron gas. **Physical Review** 136: B864.
- Kittel, C. (1996). **Introduction to Solid State Physics**. United State of America: Cambridge University. John Wiley & Sons, Inc.
- Kohn, W. and Sham, L. J. (1965). Self-Consistent equations including exchange and correlation effects. **Physical Review** 140: A1133.
- Kresse, G. and Furthmüller, J. (1996). Efficient iterative schemes for *ab initio* total-energy calculations using a plane-wave basis set. **Physical Review B** 54: 11169.
- Lheureux, D., Fischer, M., Polian, A., Itie, J. P., Gauthier, M. and Syfosse, G. (1999) Elastic properties of SrTiO₃ under extreme conditions: A new high pressure ultrasonic measurement set-up. In **Ultrasonics Symposium, 1999. Proceedings**. 1999 IEEE, Vol. 1, pp. 533.
- Li, Z., Chan, S. K., Grimsditch, M. H. and Zouboulis, E. S. (1991). The elastic and electromechanical properties of tetragonal BaTiO₃ single crystals. **Journal of Applied Physics** 70: 7327.

- Liu, Y., Xu, G., Song, C., Ren, Z., Han, G. and Zheng, Y. (2008). First-principles study of elastic properties in perovskite PbTiO_3 . **Materials Science and Engineering A** 472: 269.
- M.F.M. Taib, M.K. Yaakob, Amreesh Chandra, A.K. Arof and Yahya, M. Z. A. (2012). Effect of pressure on structural, electronic and elastic properties of cubic ($\text{Pm}3\text{m}$) SnTiO_3 using first principle calculation. **Advanced Materials Research** 501: 342.
- Meng, X., Wen, X. and Qin, G. (2010). DFT study on elastic and piezoelectric properties of tetragonal BaTiO_3 . **Computational Materials Science** 49: S372.
- Monkhorst, H. J. and Pack, J. D. (1976). Special points for Brillouin-zone integrations. **Physical Review B** 13: 5188.
- Perdew, J. P., Burke, K. and Ernzerhof, M. (1996). Generalized gradient approximation made simple. **Physical Review Letters** 77: 3865.
- Perdew, J. P. and Zunger, A. (1981). Self-interaction correction to density-functional approximations for many-electron systems. **Physical Review B** 23: 5048.
- Poindexter, E. and Giardini, A. A. (1958). Elastic constants of strontium titanate (SrTiO_3). **Physical Review** 110: 1069.
- Schranz, W., Sondergeld, P., Kityk, A. V. and Salje, E. K. H. (1999). Elastic properties of SrTiO_3 crystals at ultralow frequencies. **Phase Transitions** 69: 61.
- Wang, J. J., Meng, F. Y., Ma, X. Q., Xu, M. X. and Chen, L. Q. (2010). Lattice, elastic, polarization, and electrostrictive properties of BaTiO_3 from first-principles. **Journal of Applied Physics** 108: 034107.

Wolfram Quester Source (2013). [On-line] Available:

http://en.wikipedia.org/wiki/File:Periodic_table.png.



CHAPTER VI

CONCLUSIONS AND FUTURE RESEARCH

6.1 Conclusions

In this thesis, elastic properties of selected perovskite oxides materials, namely BeTiO_3 , MgTiO_3 , CaTiO_3 , SrTiO_3 , BaTiO_3 , PbTiO_3 , PbZrO_3 and PbHfO_3 were calculated by utilizing first principles method. The pressure dependencies of their elastic properties and sound velocities were calculated for some of the aforementioned materials. The effects of cation species on the elastic constants were also studied and analyzed. The main results from our study can be summarized as follows:

The elastic constants and sound velocities of the cubic phase of PbTiO_3 and PbZrO_3 as functions of the pressure were investigated based on first principles calculations. Under ambient conditions, our calculated elastic properties of both materials are in good agreement with available experimental results. The calculated LDA lattice constants are smaller than the ones obtained by GGA while the LDA elastic constants are larger than the ones obtained by GGA which is consistent with what have been observed in other materials and available literatures. The elastic constants and sound velocities were also studied under the pressure range of 0 – 40 GPa. All elastic constants almost linearly increase with pressure in this range. C_{11} elastic constant rapidly increases with pressure while C_{12} and C_{44} are found to be less

sensitive to pressure. Because the sound velocities are related to the elastic constants, almost all of them also increase with pressure (Pandech *et al.*, 2013).

The trends of how elastic constants changed with cation species were studied. The elastic constants of the cubic phase of perovskite $ATiO_3$ ($A = Be, Mg, Ca, Sr$ and Ba) and $PbBO_3$ ($B = Ti, Zr$ and Hf) were systematically studied for this purpose. The maximum C_{11} elastic constant is found when the atomic size of the cations at the A-site and B-site are comparable. This was explained by the nature of the perovskite crystal structure that allows both types of cations to contribute to the stiffness of the crystal when they are comparable in size and only one type is dominated when the size of the cations are different. C_{12} elastic constant is mainly defined by the oxygen cage, when Ti is at the center, and is not very sensitive to the A-site cations. When the B-site cation is changed from Ti to a larger size cations, C_{12} slightly decreases due to weaker oxygen cages. For $ATiO_3$, C_{44} elastic constant increases with the size of A-site cations. For $PbBO_3$, C_{44} slightly decreases with the size of B-site cations. This is because the cube structure defined by the A-site cations plays a major role in the shear elastic. When A-site cations are relatively large compare to the B-site cations, the cube structure maintains its high integrity. As the B-site cations turns larger the cube is forced to expand making it easier to shear.

6.2 Future Research Plan

Extension of the study of the elastic properties and sound velocities of aforementioned materials to more complicated crystal structures such as tetragonal, orthorhombic, rhombohedral, and etc. are suggested. The calculations of elastic constants and sound velocities could be performed using the same approach described

in Chapter III. However, the number of independent elastic constants is now more than three (for cubic) due to the reduced symmetry of the crystal structures. For example, there are six independent elastic constants of tetragonal structure and nine independent elastic constants of orthorhombic structure (Tinder, 2008).

As mentioned in Chapter III, the general form of the elastic constants matrix contains 36 components (Equation 3.3). For materials with crystal symmetries, the number of elastic constants can be reduced based on the level of symmetries. For the case of tetragonal structure, the 36 elastic constants can be reduced to only 6 independent elastic constants. The elastic constants matrix for a tetragonal crystal has the form (Kittel, 1996; Tinder, 2008)

$$\begin{pmatrix} C_{11} & C_{12} & C_{13} & 0 & 0 & 0 \\ C_{12} & C_{11} & C_{13} & 0 & 0 & 0 \\ C_{13} & C_{13} & C_{33} & 0 & 0 & 0 \\ 0 & 0 & 0 & C_{44} & 0 & 0 \\ 0 & 0 & 0 & 0 & C_{44} & 0 \\ 0 & 0 & 0 & 0 & 0 & C_{66} \end{pmatrix}. \quad (6.1)$$

We have calculated the structural parameters and elastic constants of selected oxides in the tetragonal perovskite structure. The structure of an ideal tetragonal structure used in our calculations is illustrated in Figure 6.1. The equivalent positions of the atoms are shown in Table 6.1. Our calculated values of lattice parameters and elastic constants are shown in Table 6.2 in comparison with available calculated and experimental results in the literatures. Our calculated values are in reasonable agreement with the literatures.

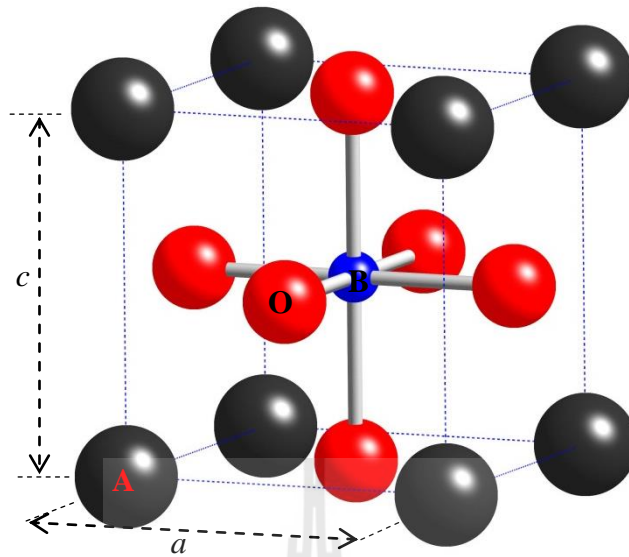


Figure 6.1 An ideal tetragonal perovskite unit cell. The dark gray spheres represent *A* cations, blue spheres: *B* cation, and red spheres: oxygen anions.

Table 6.1 Atomic positions in the ideal tetragonal perovskite structure.

Site	Location	Co-ordinations
<i>A</i> cation	(2a)	(0, 0, 0)
<i>B</i> cation	(2a)	(0.5, 0.5, 0.5)
O anion	(6b)	(0.5, 0.5, 0) (0.5, 0, 0.5) (0, 0.5, 0.5)

Table 6.2 Lattice parameters and elastic constants for selected oxides in the tetragonal perovskite structure. Values in parentheses are from the literature.

Lattice parameters	Compounds								
	BaTiO ₃			PbTiO ₃			SnTiO ₃		
	LDA	GGA	Expt.	LDA	GGA	Expt.	LDA	GGA	Expt.
a (Å)	3.95 (3.96 ^a)	4.03 (3.984 ^b)	(3.992 ^c)	3.82 (3.86 ^e)	3.89	(3.904 ^f)	3.76 (3.78 ^h)	3.83 (3.85 ^h)	(3.8 ⁱ)
c (Å)	4.05 (4.03 ^a)	4.19 (4.066 ^b)	(4.036 ^c)	3.96 (4.02 ^e)	4.02	(4.157 ^f)	3.98 (4.27 ^h)	4.08 (4.4 ^h)	(4.14 ⁱ)
c/a	1.03 (1.02 ^a)	1.04 (1.021 ^b)	(1.011 ^c)	1.04 (1.04 ^e)	1.03	(1.065 ^f)	1.06 (1.13 ^h)	1.07 (1.15 ^h)	(1.09 ⁱ)
V (Å ³)	62.2 (63.5 ^a)	68.1 (64.537 ^b)	(64.32 ^c)	58.8	62.4	(63.4 ^f)	58.5	62.1	(59.78 ⁱ)
Elastic constants									
C_{11}	347 (300 ^a)	276 (254.8 ^b)	(222 ^d)	460 (339 ^e)	379.2	(235 ^g)	503	427	-
C_{12}	128 (109 ^a)	108 (101.4 ^b)	(134 ^d)	165 (140 ^e)	145.4	(101 ^g)	171	153	-
C_{13}	123 (90 ^a)	102 (104.1 ^b)	(111 ^d)	150 (143 ^e)	131.1	(98.8 ^g)	150	134	-
C_{33}	299 (149 ^a)	203 (158.5 ^b)	(151 ^d)	354 (323 ^e)	268	(105 ^g)	340	267	-
C_{44}	126 (124 ^a)	111 (68 ^b)	(61.1 ^d)	107 (107 ^e)	98.1	(65.1 ^g)	94	89	-
C_{66}	128 (128 ^a)	111 (118.6 ^b)	(134 ^d)	106 (109 ^e)	96.6	(104 ^g)	92	87	-

^aCalculations by Wang *et al.* (Wang *et al.*, 2010)

^bCalculations by Meng *et al.* (Meng *et al.*, 2010)

^cMeasurement by Kwei *et al.* (Kwei G. H. *et al.*, 1993)

^dMeasurement by Khalal *et al.* (Khalal *et al.*, 1999)

^eCalculations by Liu *et al.* (Liu *et al.*, 2008)

^fMeasurement by Kuroiwa *et al.* (Kuroiwa *et al.*, 2001)

^gMeasurement by Li *et al.* (Li *et al.*, 1996)

^hCalculations by Parker *et al.* (Parker *et al.*, 2011)

ⁱMeasurement by Matar *et al.* (Matar *et al.*, 2009)

In the future, we are planning to study the elastic constants and sound velocities of tetragonal perovskite oxides under pressure using the similar approach we employed for the cubic case.

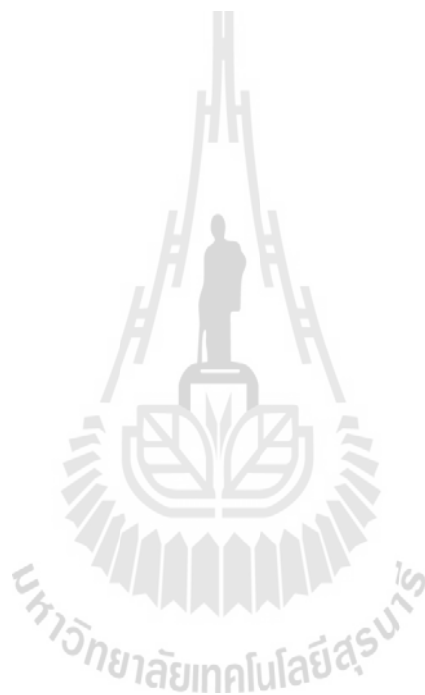
This thesis shows that the first principles calculation can be used reliably to study the elastic properties and sound velocities of materials with the illustration of several perovskite oxide systems. The approaches illustrated in this thesis can be applied to study other materials as well.

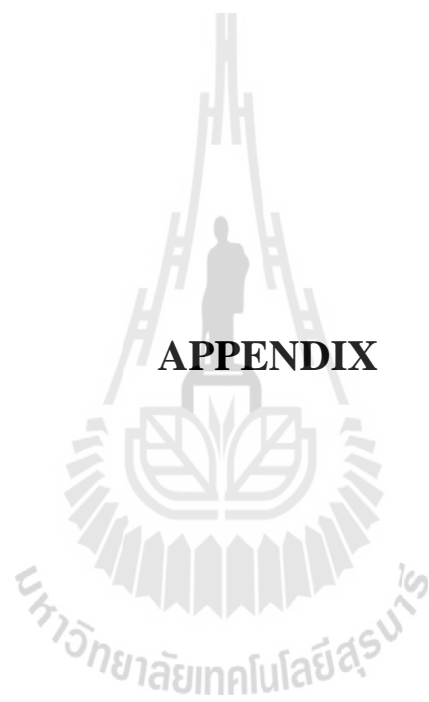
6.3 References

- Khalal, A., Khatib, D. and Jannot, B. (1999). Elastic and piezoelectric properties of BaTiO₃ at room temperature. **Physica B: Condensed Matter** 271: 343.
- Kittel, C. (1996). **Introduction to Solid State Physics**. United State of America: Cambridge University. John Wiley & Sons, Inc.
- Kresse, G. and Furthmüller, J. (1996). Efficiency of *ab-initio* total energy calculations for metals and semiconductors using a plane-wave basis set. **Computational Materials Science** 6: 15.
- Kresse, G. and Hafner, J. (1994). Norm-conserving and ultrasoft pseudopotentials for first-row and transition elements. **Journal of Physics: Condensed Matter** 6: 8245.
- Kuroiwa, Y., Aoyagi, S., Sawada, A., Harada, J., Nishibori, E., Takata, M. and Sakata, M. (2001). Evidence for Pb-O covalency in tetragonal **Physical Review Letters** 87: 217601.

- Kwei G. H. , Lawson A. C. , Billinge S. J. L. and Cheong S. W (1993). Structures of the ferroelectric phases of barium titanate. **The Journal of Physical Chemistry** 97: 2368.
- Li, Z., Grimsditch, M., Foster, C. M. and Chan, S. K. (1996). Dielectric and elastic properties of ferroelectric materials at elevated temperature. **Journal of Physics and Chemistry of Solids** 57: 1433.
- Liu, Y., Xu, G., Song, C., Ren, Z., Han, G. and Zheng, Y. (2008). First-principles study of elastic properties in perovskite PbTiO_3 . **Materials Science and Engineering A** 472: 269.
- Matar, S. F., Baraille, I. and Subramanian, M. A. (2009). First principles studies of SnTiO_3 perovskite as potential environmentally benign ferroelectric material. **Chemical Physics** 355: 43.
- Meng, X., Wen, X. and Qin, G. (2010). DFT study on elastic and piezoelectric properties of tetragonal BaTiO_3 . **Computational Materials Science** 49: S372.
- Pandech, N., Sarasamak, K. and Limpijumnong, S. (2013). Sound velocities and elastic properties of PbTiO_3 and PbZrO_3 under pressure: First principles study. **Ceramics International** 39, Supplement 1: S277.
- Parker, W. D., Rondinelli, J. M. and Nakhmanson, S. M. (2011). First-principles study of misfit strain-stabilized ferroelectric SnTiO_3 . **Physical Review B** 84: 245126.
- Tinder, F. R. (2008). **Tensor Properties of Solids: Phenomenological Development of the Tensor Properties of Crystals**. Morgan & Claypool.

Wang, J. J., Meng, F. Y., Ma, X. Q., Xu, M. X. and Chen, L. Q. (2010). Lattice, elastic, polarization, and electrostrictive properties of BaTiO₃ from first-principles. **Journal of Applied Physics** 108: 157.





APPENDIX

APPENDIX

PUBLICATIONS AND PRESENTATIONS

1. List of publications

Pandech, N., Sarasamak, K. and Limpijumnong, S. (2013). Sound velocities and elastic properties of PbTiO_3 and PbZrO_3 under pressure: First principles study. **Ceramics International** 39, Supplement 1: S277.

2. List of oral presentations

Pandech, N., Sarasamak, K., and Limpijumnong, S. (May 2012). Elastic Properties of PbTiO_3 Under Pressure. In **Siam Physics Congress 2012**. Ayuttaya, Thailand: Thai Physics Society.

Pandech, N., Sarasamak, K., and Limpijumnong, S. (April 2013). Elastic Properties of ATiO_3 (A= Be, Mg, Ca, Sr and Ba): First- Principles Calculations. In **Siam Physics Congress 2013**. Chaingmai, Thailand: Thai Physics Society.

Pandech, N., Sarasamak, K., and Limpijumnong, S. (July 2013). Elastic Properties of Selected Perovskite Materials: First-Principles Study. In **A special seminar at Technische Universität Darmstadt**. Darmstadt, Germany.

3. List of poster presentations

Pandech, N., Sarasamak, K., and Limpijumnong, S. (July 2012). Sound Velocities and Elastic Properties of PbTiO_3 and PbZrO_3 Under Pressure: First Principles Study. In **The 8th Asian Meeting on Electroceramics (AMEC-8)**. Penang, Malaysia.

Schwertfager, N., Pandech, N., and Limpijumnong, S. (December 2012). Calculated X-ray absorption of cation-off centering in $\text{Bi}(\text{Mg}_{1/2}\text{Ti}_{1/2})\text{O}_3$. In **The 8th Asian Meeting on Ferroelectric (AMF-8)**. Pattaya, Thailand.

Pandech, N., Sarasamak, K., and Limpijumnong, S. (July 2013). Elastic Properties of Perovskite ATiO_3 (A= Be, Mg, Ca, Sr and Ba) and PbBO_3 (B= Ti, Zr, and Hf): First Principles Calculation. In **The 7th Conference of the Asian Consortium on Computational Materials Science (ACCMS-7)**. Nakhon Ratchasima, Thailand.

Pandech, N., Sarasamak, K., and Limpijumnong, S. (November 2013). Elastic parameters of PbTiO_3 from first principles calculations. In **The 3rd Academic Conference on Natural Science for Master and PhD Students from ASEAN Countries**. Phnom Penh, Cambodia.

Available online at www.sciencedirect.com

SciVerse ScienceDirect

Ceramics International 39 (2013) S277–S281

CERAMICS
INTERNATIONALwww.elsevier.com/locate/ceramint

Sound velocities and elastic properties of PbTiO_3 and PbZrO_3 under pressure: First principles study

Narasak Pandech^{a,b}, Kanoknan Sarasamak^c, Sukit Limpijumng^{a,b,*}^aSchool of Physics, Suranaree University of Technology, Nakhon Ratchasima 30000, Thailand^bThailand Center of Excellence in Physics (ThEP Center), Commission on Higher Education, Bangkok 10400, Thailand^cCollege of Nanotechnology, King Mongkut's Institute of Technology Ladkrabang, Bangkok 10520, Thailand

Available online 16 October 2012

Abstract

The elastic constants and sound velocities as a function of pressure for perovskite materials PbTiO_3 (PTO) and PbZrO_3 (PZO) were investigated by first principles calculations. Under ambient pressure, the calculated structural parameters were calculated and found to be in good agreement with known values. To study properties under pressure, PTO and PZO were calculated at several reduced volumes, each of which corresponds to the system under pressure. The C_{11} , C_{12} and C_{44} elastic constants are all found to increase with pressure for the pressure range studied. Because the sound velocities are directly derived from the elastic constants, the relationships between the sound velocities and pressure also follow similar trends. The longitudinal modes are all larger than those of the transverse modes.

© 2012 Elsevier Ltd and Techna Group S.r.l. All rights reserved.

Keywords: D. Perovskite; First principles; Sound velocities

1. Introduction

PbZrO_3 (PZO) and PbTiO_3 (PTO) are the parent compound materials of the extensively utilized ferroelectric material $\text{Pb}(\text{Ti,Zr})\text{O}_3$ (PZT). PZT (as well as PZO and PTO) has perovskite structure and is used in many devices such as ultrasonic transducers and piezoelectric actuators [1]. The room temperature phase of PZO and PTO is orthorhombic and tetragonal structure, respectively [2,3]. Both orthorhombic PZO and tetragonal PTO have only slight distortion from the perfect cubic perovskite structure. Their elastic properties have been studied by several research groups. Liu et al. [4] theoretically studied the elastic properties of PTO in both cubic and tetragonal phases. Kalinichev et al. [3] used Brillouin light scattering to obtain the elastic and piezoelectric constants for tetragonal PTO single crystals at room temperature. For PZO,

Kagimura and Singh [2] studied the elastic properties and energetics of orthorhombic and rhombohedral phases.

Some effects of hydrostatic pressures on perovskite materials beside PTO and PZO have been experimentally and theoretically investigated. To our knowledge, the elastic properties and sound velocities of PTO and PZO under pressure have not been reported. For PTO, most of previous works were performed in order to understand their ferroelectric properties under ambient pressure. Liu et al. [4] focused mainly on the calculations of equilibrium tetragonal to cubic phase transition pressure of PTO. In this work, the elastic constants and sound velocities under pressure in cubic perovskite PZO and PTO were studied by using the density functional theory calculations.

2. Elastic properties of the cubic perovskite crystal

2.1. Elastic constants of the cubic perovskite crystal

Elastic constants of materials can be obtained by *ab-initio* calculations using two main approaches [5]. The first approach is based on the analysis of the total energies of the strained state of the materials which is

*Corresponding author at: School of Physics, Suranaree University of Technology, Nakhon

Ratchasima 30000, Thailand. Tel.: +66 4422 3000.

E-mail address: sukit@sut.ac.th (S. Limpijumng).

called “energy strain approach” [6]. Another approach is based on the analysis of the changes in calculated stress values resulting from the changes in the strain. This approach is called “stress strain approach” [7].

In this work, the elastic constants (C_{ij}) were calculated by using the stress strain approach. The stress strain relation can be written in the matrix form as

$$\begin{pmatrix} \sigma_{xx} \\ \sigma_{yy} \\ \sigma_{zz} \\ \sigma_{yz} \\ \sigma_{zx} \\ \sigma_{xy} \end{pmatrix} = \begin{pmatrix} C_{11} & C_{12} & C_{13} & C_{14} & C_{15} & C_{16} \\ C_{21} & C_{22} & C_{23} & C_{24} & C_{25} & C_{26} \\ C_{31} & C_{32} & C_{33} & C_{34} & C_{35} & C_{36} \\ C_{41} & C_{42} & C_{43} & C_{44} & C_{45} & C_{46} \\ C_{51} & C_{52} & C_{53} & C_{54} & C_{55} & C_{56} \\ C_{61} & C_{62} & C_{63} & C_{64} & C_{65} & C_{66} \end{pmatrix} \begin{pmatrix} e_{xx} \\ e_{yy} \\ e_{zz} \\ e_{yz} \\ e_{zx} \\ e_{xy} \end{pmatrix} \quad (1)$$

where σ_{ij} ($i, j = x, y, z$) are the stress components, e_{ij} ($i, j = x, y, z$) are the strain components, and $C_{\lambda\alpha}$ ($\lambda, \alpha = 1, 2, 3, \dots, 6$) are the elastic constants. For cubic perovskite structure, the 36 elastic constants in Eq. (1) can be reduced to three independent elastic constants because of the high symmetry of the structure. The three independent elastic constants are denoted by C_{11} , C_{12} and C_{44} . Eq. (1) is reduced to

$$\begin{pmatrix} \sigma_{xx} \\ \sigma_{yy} \\ \sigma_{zz} \\ \sigma_{yz} \\ \sigma_{zx} \\ \sigma_{xy} \end{pmatrix} = \begin{pmatrix} C_{11} & C_{12} & C_{12} & 0 & 0 & 0 \\ C_{12} & C_{11} & C_{12} & 0 & 0 & 0 \\ C_{12} & C_{12} & C_{11} & 0 & 0 & 0 \\ 0 & 0 & 0 & C_{44} & 0 & 0 \\ 0 & 0 & 0 & 0 & C_{44} & 0 \\ 0 & 0 & 0 & 0 & 0 & C_{44} \end{pmatrix} \begin{pmatrix} e_{xx} \\ e_{yy} \\ e_{zz} \\ e_{yz} \\ e_{zx} \\ e_{xy} \end{pmatrix} \quad (2)$$

2.2. Sound velocities of the cubic perovskite crystal

Sound velocities in materials are related to their elastic constants by a simple relationship:

$$v_P(\hat{q}) = \sqrt{C_P(\hat{q})/\rho} \quad (3)$$

where P indicates the polarization, which can be either L for longitudinal or T for transverse, and \hat{q} is the propagation direction of the wave. ρ is the mass density and $C_k(\hat{q})$

is the combination of elastic constants. The expression on the right hand side of Eq. (3) for three propagation directions of the cubic perovskite structure are summarized in Table 1.

3. Computational method

The computational approach employed was based on first principles density functional theory [8,9] with the plane wave pseudo-potential as implemented in Vienna *Ab-initio* Simulation Package (VASP) code [10]. For the exchange correlation terms, both local density approximation (LDA) [11,12] and generalized gradient approximation (GGA) [13] were used. The ultrasoft version of the pseudo-potential implemented in the VASP code allows a low cut off energies for the plane wave expansion of only 500 eV. We used a $8 \times 8 \times 8$ Monkroost Pack scheme [14] k -point sampling.

A cubic perovskite structure has the space group $Pm\bar{3}m(\#221)$ with the Wychoff positions: Pb 1a (0,0,0), Ti (or Zr) 1b (0.5,0.5,0.5) and O 3c (0,0.5,0.5), (0.5,0.5,0) and (0.5,0,0.5) as illustrated in Fig. 1.

The total energies (E) of a unit cell of the crystal at several slightly different volumes (V) were calculated and fitted into the equation of states [15] to obtain the bulk modulus (B_0) and its pressure derivative (B') of the crystal. In order to study the crystal properties under pressures, the elastic constants and sound velocities were calculated at several reduced volumes, following the approach described in Ref. [16]. The reduced crystal volume can be translated into the corresponding pressure following pressure volume (P – V) relationship in the Birch–Murnaghan's equation of state [17] written as

$$P(V) = \frac{3B_0}{2} \left[\left(\frac{V_0}{V} \right)^{7/3} - \left(\frac{V_0}{V} \right)^{5/3} \right] \left\{ 1 + \frac{3}{4}(B'-4) \left[\left(\frac{V_0}{V} \right)^{2/3} - 1 \right] \right\} \quad (4)$$

where V_0 is the equilibrium volume.

Table 1
Sound velocity expressions of each wave propagation direction for the cubic structure.

Sound velocity	Expression
$v_L([100])$	$(C_{11}/\rho)^{1/2}$
$v_T([100])$	$(C_{44}/\rho)^{1/2}$
$v_L([110])$	$[(C_{11} + C_{12} + 2C_{44})/2\rho]^{1/2}$
$v_T([110])$	$[(C_{11} - C_{12})/\rho]^{1/2}$
$v_L([111])$	$[(C_{11} + 2C_{12} + 4C_{44})/3\rho]^{1/2}$
$v_T([111])$	$[(C_{11} - C_{12} + C_{44})/3\rho]^{1/2}$

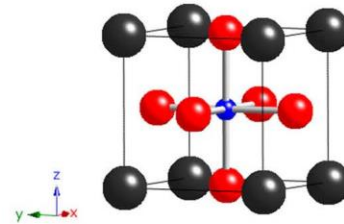


Fig. 1. Schematic illustration of a cubic perovskite unit cell. The dark gray spheres represent Pb atoms, blue sphere: Ti or Zr atom and red spheres: O atoms. (For interpretation of the references to color in this figure legend, the reader is referred to the web version of this article.)

4. Results and discussions

4.1. Structural and elastic properties at zero pressure

The calculated equilibrium lattice constants as well as the corresponding volumes of both PTO and PZO based on both LDA and GGA exchange correlation functional are compared to other computation and experimental results in Table 2. Our values are consistent with other calculated results. In comparison with the experimental values, LDA tends to give slightly too small lattice constants while GGA tends to give slightly too large values. This is consistent with what have been observed in other materials.

The bulk modulus (B), its pressure derivative (B') and the elastic constants at zero pressure of both PTO and PZO are also shown in Table 2. Because LDA gives smaller lattice constants compared to GGA, the bulk moduli and all elastic constants computed using LDA are consistently higher than those corresponding ones computed using GGA. PTO has been previously studied by Piskunov et al. [18] and Liu et al. [4]. Liu et al. values calculated based on LDA are very similar to ours. However, Piskunov et al. LDA results are consistently higher

than ours while their GGA results are quite similar. To our knowledge, there is no computation result available for PZO. The sound velocities, shown in the bottom section of Table 2, can be derived from the elastic constants using the expressions shown in Table 1.

4.2. Elastic properties under pressure

To study the elastic constants and sound velocities under hydrostatic pressures, the calculations were performed at several reduced volumes, each of which corresponds to the system under a different pressure. The pressure can be determined from the pressure volume relation shown by Eq. (1). Sound velocities of PTO and PZO under pressure can be obtained from the corresponding elastic constants using the expressions given in Table 1.

The elastic constants as a function of pressure for cubic perovskite PTO and PZO are shown in Fig. 2. Both materials have similar behavior in the changes of elastic constants under pressure. In general, we can see that all three elastic constants, C_{11} , C_{12} and C_{44} increase with pressure. In both PTO and PZO, C_{11} , which is related to the longitudinal distortion, rapidly increases with pressure. On the other hand, C_{12} and C_{44} are much less sensitive to

Table 2

Calculated lattice constants (a) in Å, volumes (V_0) in Å³, bulk modulus (B) in GPa, its pressure derivative (B'), elastic constants in GPa and sound velocities in km/s of PbTiO₃ and PbZrO₃ in the cubic perovskite structure compared with literatures.

		PbTiO ₃		PbZrO ₃	
		LDA	GGA	LDA	GGA
a	Present	3.89	3.97	4.13	4.20
	Other calc.	3.88 ^a , 3.93 ^b	3.98 ^a , 3.96 ^b	4.11 ^c	4.19 ^c , 4.18 ^d
	Expt.	3.95 ^e		4.16 ^f	
V_0	Present	58.76	63.32	70.22	74.08
B	Present	219	185	181	168
	Other calc.	229 ^g , 324 ^h	213 ^b	–	–
B'	Present	4.5	3.5	4.6	3.7
C_{11}	Present	380	316	366	322
	Other calc.	384 ^g , 450 ^h	325 ^b	–	–
C_{12}	Present	145	130	92	89
	Other calc.	151 ^g , 261 ^h	158 ^b	–	–
C_{44}	Present	103	96	63	62
	Other calc.	120 ^g , 113 ^h	107 ^b	–	–
$v_L[100]$	Present	6.66	6.25	6.69	6.42
$v_T[100]$	Present	3.46	3.44	2.78	2.82
$v_L[110]$	Present	6.53	6.28	5.98	5.86
$v_T[110]$	Present	3.70	3.39	4.10	3.86
$v_L[111]$	Present	6.48	6.43	5.72	5.65
$v_T[111]$	Present	3.63	3.55	3.71	3.55

^aCalculations by Hosseini et al. [19].

^bCalculations by Piskunov et al. [18].

^cCalculations by Wang et al. [20].

^dCalculations by Baedi et al. [21].

^eMeasurements by Kuroiwa et al. [22].

^fMeasurements by Fujiishita et al. [23].

^gCalculations by Liu et al. [4].

S280

N. Pandey et al. / Ceramics International 39 (2013) S277–S281

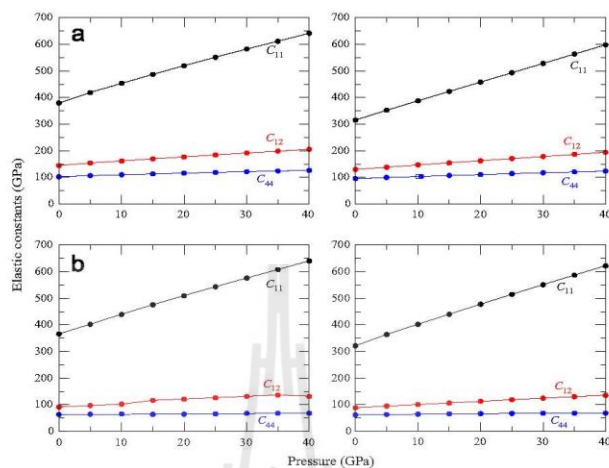


Fig. 2. Elastic constants as a function of pressure for cubic perovskite PbTiO_3 and PbZrO_3 , obtained from LDA (left) and GGA (right). (a) PbTiO_3 and (b) PbZrO_3 .

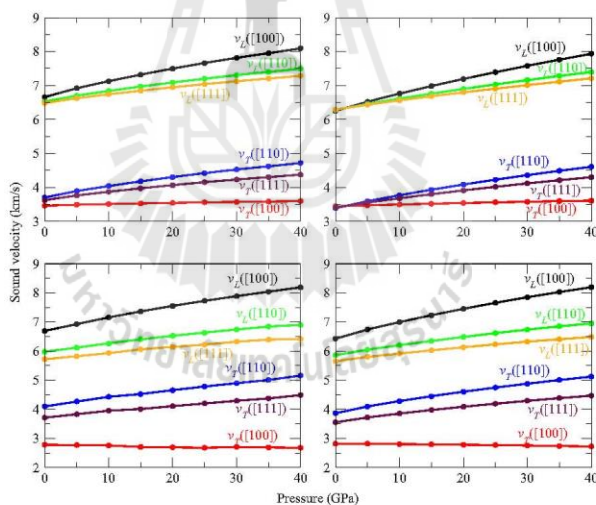


Fig. 3. Sound velocities as a function of pressure for cubic perovskite PbTiO_3 and PbZrO_3 , obtained from LDA (left) and GGA (right). (a) PbTiO_3 and (b) PbZrO_3 .

pressure. Indeed, C_{44} , which is related to the transverse distortion, remains almost flat. The calculated sound velocities under pressure for both cubic perovskite PTO and PZO are shown in Fig. 3. Since the sound velocities are directly derived from the elastic constants, a similar

trend was found. All of the sound velocities, except for the $v_T(100)$ of PZO, increase with pressure mainly because they contain C_{11} which rapidly increases with pressure. In PZO, $v_T(100)$ slightly decreases under pressure because it is associated only with C_{44} which remains almost flat

with pressure and divided by ρ which increases with pressure. As expected, the longitudinal modes are larger than the transverse modes such that they can be divided into two groups.

5. Conclusions

The elastic constants and sound velocities of perovskite PTO and PZO as a function of pressure were calculated by first principles calculations. Both LDA and GGA exchange and correlations were used. The calculated zero-pressure properties are in good agreement with the previous studies ensuring the validity of the results. LDA gives slightly smaller lattice constants and larger bulk moduli than GGA which is consistent with what have been observed in other materials. The elastic constants and sound velocities under the pressure range of 0–40 GPa were presented. The elastic constants are almost linearly increased with pressure. C_{11} rapidly increases with pressure while C_{12} and C_{44} are much less sensitive to pressure. Because the sound velocities are related to the elastic constants, almost all of them increase with pressure.

Acknowledgments

This work was partially supported by Development and Promotion of Science and Technology Talents Project (DPST, Thailand) and Thailand Center of Excellence in Physics (ThEP Center). Computations were carried out at the Synchrotron Light Research Institute, Thailand.

References

- [1] T. Yamamoto, Y. Makino, Pressure dependence of ferroelectric properties in PbZrO_3 – PbTiO_3 solid state system under hydrostatic stress, *Japanese Journal of Applied Physics* 35 (1996) 3214–3217.
- [2] R. Kagimura, D.J. Singh, First-principles investigations of elastic properties and energetics of antiferroelectric and ferroelectric phases of PbZrO_3 , *Physical Review B* 77 (2008) 104113.
- [3] A.G. Kalimichev, J.D. Bass, B.N. Sun, D.A. Payne, Elastic properties of tetragonal PbTiO_3 single crystals by Brillouin scattering, *Journal of Materials Research* 12 (1997) 2623–2627.
- [4] Y. Liu, G. Xu, C. Song, Z. Ren, G. Han, Y. Zheng, First-principles study of elastic properties in perovskite PbTiO_3 , *Materials Science and Engineering A: Structural Materials, Properties, Microstructure and Processing* 472 (2008) 269–272.
- [5] Y. Le Page, P. Saxe, Symmetry-general least-squares extraction of elastic data for strained materials from ab initio calculations of stress, *Physical Review B* 65 (2002) 104104.
- [6] Y. Le Page, P. Saxe, Symmetry-general least-squares extraction of elastic coefficients from ab initio total energy calculations, *Physical Review B* 63 (2001) 174103.
- [7] O.H. Nielsen, R.M. Martin, First-principles calculation of stress, *Physical Review Letters* 50 (1983) 697–700.
- [8] P. Hohenberg, W. Kohn, Inhomogeneous electron gas, *Physical Review* 136 (1964) B864–B871.
- [9] W. Kohn, L.J. Sham, Self-consistent equations including exchange and correlation effects, *Physical Review* 140 (1965) A1133–A1138.
- [10] G. Kresse, J. Furthmüller, Efficient iterative schemes for ab initio total-energy calculations using a plane-wave basis set, *Physical Review B* 54 (1996) 11169–11186.
- [11] D.M. Ceperley, B.J. Alder, Ground state of the electron gas by a stochastic method, *Physical Review Letters* 45 (1980) 566–569.
- [12] J.P. Perdew, A. Zunger, Self-interaction correction to density-functional approximations for many-electron systems, *Physical Review B* 23 (1981) 5048–5079.
- [13] J.P. Perdew, K. Burke, M. Ernzerhof, Generalized gradient approximation made simple, *Physical Review Letters* 77 (1996) 3865–3868.
- [14] H.J. Monkhorst, J.D. Pack, Special points for Brillouin-zone integrations, *Physical Review B* 13 (1976) 5188–5192.
- [15] J.H. Li, S.H. Liang, H.B. Guo, B.X. Liu, Four-parameter equation of state of solids, *Applied Physics Letters* 19 (2005) 194111–194113.
- [16] K. Sarasamak, S. Limpjumnong, W.R.L. Lambrecht, Pressure-dependent elastic constants and sound velocities of wurtzite SiC , GaN , InN , ZnO , and CdSe , and their relation to the high-pressure phase transition: a first-principles study, *Physical Review B* 82 (2010) 035201.
- [17] J.P. Poirier, *Introduction to the Physics of the Earth Interior*, second ed., Cambridge University Press, Cambridge, 2000.
- [18] S. Piskunov, E. Heifets, R.I. Eglitis, G. Borstel, Bulk properties and electronic structure of SrTiO_3 , BaTiO_3 , PbTiO_3 perovskites: an ab initio HF/DFT study, *Computational Materials Science* 29 (2004) 165–178.
- [19] S.M. Hosseini, T. Movlaroooy, A. Kompany, First-principle calculations of the cohesive energy and the electronic properties of PbTiO_3 , *Physica B* 391 (2007) 316–321.
- [20] Y.X. Wang, M. Arai, T. Sasaki, C.L. Wang, W.L. Zhong, First-principles study on the (001) surface of cubic PbZrO_3 and PbTiO_3 , *Surface Science* 585 (2005) 75–84.
- [21] J. Baedi, S.M. Hosseini, A. Kompany, E.A. Kakhki, Structural, electronics and optical properties of lead zirconate, *Physica Status Solidi B* 245 (2008) 2572–2580.
- [22] Y. Kuroiwa, S. Aoyagi, A. Sawada, J. Harada, E. Nishibori, M. Takata, M. Sakata, Evidence for Pb–O covalency in tetragonal PbTiO_3 , *Physical Review Letters* 87 (2001) 217601–217604.
- [23] H. Fujishita, Y. Ishikawa, S. Tanaka, A. Ogawaguchi, S. Katano, Crystal structure and order parameters in the phase transition of antiferroelectric PbZrO_3 , *Journal of the Physical Society of Japan* 72 (2002) 1426–1435.

Abstract presented at the Siam Physics Congress 2012

Phra Nakhon Si Ayuttaya, Thailand (2012)

Siam Physics Congress SPC2012
Past, Present and Future of Physics 9-12 May 2012

Elastic Properties of PbTiO_3 Under Pressure

N. Pandech^{1,2*}, K. Sarasamak³ and S. Limpijumnong^{1,2}

¹*School of Physics, Suranaree University of Technology and Synchrotron Light Research Institute, Nakhon Ratchasima 30000, Thailand*

²*Thailand Center of Excellence in Physics (ThEP Center), Commission on Higher Education, Bangkok 10400, Thailand*

³*College of KMITL Nanotechnology, King Mongkut's Institute of Technology Ladkrabang, Bangkok 10520, Thailand*

*Corresponding author. E-mail: na_ra_suk@hotmail.com

Abstract

The elastic constants as a function of pressure for perovskite materials PbTiO_3 (PTO) were studied by first principles density functional calculations as implemented in Vienna Ab-initio Simulation Package (VASP). Both local density approximation (LDA) and generalized gradient approximation (GGA) were employed and compared. At zero pressure (the results are also applied for ambient pressure conditions), the calculated fully relaxed structure of PTO is in good agreement with known experimental results. The elastic constants at zero pressure are in reasonable agreement with the known literature. To study the properties under different pressure condition, we calculated PTO properties at several reduced volumes. The equation of state curve is then used to relate each compressed volume to the corresponding hydrostatic pressure. The C_{11} , C_{12} and C_{44} elastic constants are all found to increase monotonically with the pressure for the pressure range studied.

Keywords: PbTiO_3 , perovskite, elastic constants, first principles

Abstract presented at the Siam Physics Congress 2013

Chiang Mai, Thailand (2013)

Siam Physics Congress SPC2013
 Thai Physics Society on the Road to ASEAN Community 21-23 March 2013

Elastic Properties of Perovskite $ATiO_3$ (A= Be, Mg, Ca, Sr and Ba): First-Principles Calculations

Narasak Pandech^{1,2}, Kanoknan Sarasamak³ and Sukit Limpijumnong^{1, 2*}

¹*School of Physics, Suranaree University of Technology and Synchrotron Light Research Institute, Nakhon Ratchasima, 30000 Thailand*

²*Thailand Center of Excellence in Physics (ThEP Center), Commission on Higher Education, Bangkok, 10400 Thailand*

³*College of Nanotechnology, King Mongkut's Institute of Technology Ladkrabang, Bangkok, 10520 Thailand*

*Corresponding author. E-mail: sukit@sut.ac.th

Abstract

First principles calculation based on density functional theory (DFT) was used to study the elastic properties of perovskite $ATiO_3$ (A=Be, Mg, Ca, Sr and Ba). Both local density approximation (LDA) and generalized gradient approximation (GGA) were used. The C_{11} , C_{12} and C_{44} elastic constants are studied as a function of atomic number of A-site atom. C_{11} is maximum when the atomic number of A-site atom is comparable to the atomic number of B-site atom. C_{12} is found to be quite independent with A-site atom. C_{44} is found to increase with the atomic number of A-site atom.

Keywords: First-principles, Elasticity, Perovskite

มหาวิทยาลัยเทคโนโลยีสุรนารี

Abstract presented at a special seminar at Technische Universität *Darmstadt*.

Darmstadt, Germany. (2013)

Elastic Properties of Selected Perovskite Materials: First-Principles Study

Narasak Pandech^{1,2*}, Kanoknan Sarasamak³ and Sukit Limpijumnong^{1,2}

¹ *Scholl of Physics, Suranaree University of Technology, Nakhon Ratchasima, 30000 Thailand*

² *Thailand Center of Excellence in Physics (ThEP Center), Commission on Higher Education, Bangkok, 10400 Thailand*

³ *College of Nanotechnology, King Mongkut's Institute of Technology Ladkrabang, Bangkok, 10520 Thailand*

The material research greatly enhances current knowledge on technologically sensitive materials. The knowledge allows the improvement of material syntheses as well as fabrication of new materials with desired physical properties. In modern material research, the computational technique is widely accepted to be an important tool to gain a deeper understanding of the material system under the investigation. In addition the computation techniques can be used to study the behavior of materials that are not successfully synthesized in experiments. In my thesis, the main interest is on the elastic properties and sound velocities of perovskite materials under hydrostatic pressures. I use first principles calculations based on density functional theory (DFT) with the plane wave pseudo-potential as implemented in Vienna *Ab-initio* Simulation Package (VASP). Our systematic study allows us to study the elastic properties as well as the sound velocities when the material is compressed (under hydrostatic pressures). In addition, we can also study the properties in carefully selected compounds, we can identify how the elastic constants changed with the cation species, i.e., the trend of elastic constants of ATiO_3 (A = group IIA elements) and PbBO_3 (B = Ti, Zr, and Hf) were studied and will be presented. This work illustrates how computation materials can be used to directly simulate material properties that can be measured by experiment without taking any input from experiment. The computation method we employed can provide full detail of electronic properties, vibration properties and optical properties of the system studied in addition to the physical properties shown here. Therefore the computational approach illustrated here can be used in conjunction with various experimental measurements such as infrared spectroscopy, x-ray absorption spectroscopy and UV-vis spectroscopy.

*Presenting author's email: narasakpandech@gmail.com

Abstract presented at the 8th Asian Meeting on Electroceramics (AMEC-8)

Penang, Malaysia (2012)

Sound Velocities and Elastic Properties of PbTiO₃ and PbZrO₃ Under Pressure: First Principles Study

N. Pandech^{1,2}, K. Sarasamak³ and S. Limpijumnong^{1,2}

¹*School of Physics, Suranaree University of Technology and Synchrotron Light Research Institute, Nakhon Ratchasima 30000, Thailand*

²*Thailand Center of Excellence in Physics (TheEP Center), Commission on Higher Education, Bangkok 10400, Thailand*

³*College of KMITL Nanotechnology, King Mongkut's Institute of Technology Ladkrabang, 10520 Bangkok, Thailand*

The elastic constants and sound velocities as a function of pressure for perovskite materials PbTiO₃ (PTO) and PbZrO₃ (PZO) were investigated by density functional first principles calculations. Under ambient pressure, the calculated structural parameters are in good agreement with known values. For properties under pressure, the materials (PTO and PZO) were calculated at several reduced volumes, each of which corresponds to the system under pressure. The C_{11} , C_{12} and C_{44} elastic constants are all found to increase with the pressure for the pressure range studied. Since the sound velocities is almost constant. The caused of this exception will be discussed. The sound velocities can clearly be divided into two groups; the longitudinal modes and transverse modes. The sound velocities of longitudinal modes are all larger than those of the transverse modes.

Keywords: perovskite, sound velocities, first principles

* Corresponding author's e-mail: na_ra_suk@hotmail.com

มหาวิทยาลัยเทคโนโลยีสุรนารี

Abstract presented at the 8th Asian Meeting on Ferroelectric (AMF-8)
Pattaya, Thailand (2012).

Calculated x-ray absorption spectra of cation-off centering in $\text{Bi}(\text{Mg}_{1/2}\text{Ti}_{1/2})\text{O}_3$

Nuchalee Schwertfager *, [Narasak Pandeche](#), Sukit Limpijumnong

School of Physics, Suranaree University of Technology, Nakhon Ratchasima 30000, Thailand

Recent first principles calculations [Suewattana *et al.*, Phys. Rev. B 86, 064105 (2012)] showed that Bi, Mg and Ti in $\text{Bi}(\text{Mg}_{1/2}\text{Ti}_{1/2})\text{O}_3$, hence forth BMT, are off-centering (from the center of their respective oxygen cages) much more than reported by XRD experiment [Khalyavin *et al.*, Chem. Mater 18, 5104 (2006)]. The off-centering of the cations is a characteristic of good electroactive materials. To probe the local structure of specific elements, x-ray absorption spectroscopy (XAS) is known to be a powerful technique. Here, we calculated the x-ray absorption spectra of Bi, Mg and Ti by using first-principles calculations. For each cation (Bi, Mg and Ti), the spectra were calculated for different configurations: (1) the cation is located at the center of its oxygen cage, (2) the cation is located slightly off-centered based on XRD results and (3) the cation is located largely off-centered based on the calculation results. These results show which features in XAS are affected by the shift of Bi, Mg and Ti off their respective center position. This indicates that XAS measurement would be very useful to verify the actual off-centering of cations in this material.

*Presenting author's e-mail: nuchalee.schwertfager@gmail.com



Abstract presented at the 7th Conference of the Asian Consortium on Computational Materials Science, Nakhon Ratchasima, Thailand (2013).

Elastic Properties of Perovskite $ATiO_3$ (A= Be, Mg, Ca, Sr, and Ba) and $PbBO_3$ (B= Ti, Zr, and Hf): First Principles Calculation

Narasak Pandeche^{1,2,*}, Kanoknan Sarasamak³ and Sukit Limpijumnong^{1,2}

¹ *School of Physics and NANOTEC-SUT Center of Excellence on Advanced Functional Nanomaterials, Suranaree University of Technology, Nakhon Ratchasima 30000, Thailand*

² *Thailand Center of Excellence in Physics (ThEP Center), Commission on Higher Education, Bangkok 10400, Thailand*

³ *College of Nanotechnology, King Mongkut's Institute of Technology Ladkrabang, Bangkok 10520, Thailand*

The elastic constants of several perovskite oxides were calculated by first principles approach. By systematically varied the A-site and B-site cations, the effects of cations on the elastic constants were revealed. For A-site, we fixed the B-site cation to be Ti and studied the elastic properties of perovskite $ATiO_3$ with A= Be, Mg, Ca, Sr, and Ba, one at a time. For B-site, we fixed the A-site cation to be Pb and studied the elastic properties of $PbBO_3$ (B = Ti, Zr, and Hf). We employed the density functional first principles calculations with local density approximation (LDA) and generalized gradient approximation (GGA). The C_{11} , C_{12} , and C_{44} elastic constants of above mentioned oxides were calculated and compared. For $ATiO_3$, C_{11} is maximum when the atomic number of A-site atom is comparable to that of B-site atom. C_{12} is found to be quite independent with A-site atom. C_{44} is found to increase with the atomic number of A-site atom. For $PbBO_3$, C_{11} is also maximum when the atomic number of B-site atom is comparable to the atomic number of A-site atom. There is, however, no clear relationship between C_{12} and C_{44} and the atomic number of the B-site atom.

*Presenting author's email: narasakpandeche@gmail.com

Abstract presented at The 3rd Academic Conference on Natural Science for Master and PhD Students from ASEAN Countries, Phnom Penh, Cambodia (2013).

ELASTIC PARAMETERS OF PbTiO_3 FROM FIRST PRINCIPLES CALCULATIONS

Narasak Pandech^{a,b,*}, Kanoknan Sarasamak^c and Sukit Limpijumnong^{a,b}

^{a)} School of Physics and NANOTEC-SUT Center of Excellence on Advanced Functional Nanomaterials, Suranaree University of Technology, Nakhon Ratchasima 30000, Thailand

^{b)} Thailand Center of Excellence in Physics (ThEP Center), Commission on Higher Education, Bangkok 10400, Thailand

^{c)} College of Nanotechnology, King Mongkut's Institute of Technology Ladkrabang, Bangkok 10520, Thailand

* Presenting author; E-mail: na_ra_suk@hotmail.com

Most of material properties (physical, electronics, magnetics and optical) can be studied based on the quantum mechanics calculations of the interactions between electrons and the electronic potential from the nuclei of the atoms in the material. Such calculations are called first principles calculations. In principle, one need to solve a complicated set of Schrödinger equations of a many-body system. In practice, various approximations have to be applied in order to make the computation feasible. Yet, the properties obtained are still reasonable. With today computing technology, properties of complicated crystalline compounds such as perovskite PbTiO_3 (PTO) can be study by first principles calculations using personal PC. In this presentation, we will show how the crystal parameters (the lattice constant and other internal lattice parameters) as well as elastic parameters of PTO can be calculated. Our results are in good agreement with previously reported experimental and computational results. In addition, we will show how the elastic parameters can be used to calculate sound velocities of PTO. If time permits, the extension of the calculations to study the elastic parameters and sound velocities under pressure will be presented.

Keywords: PbTiO_3 , perovskite, elastic constants, first principles

มหาวิทยาลัยเทคโนโลยีสุรนารี

CURRICULUM VITAE

Narasak Pandech was born on April 10, 1986 in Yasothon, Thailand. He received his Bachelor degree of science with the second class honor in 2008 from the Department of Physics, Faculty of Science, Khon Kaen University. In 2009, he was granted the scholarship from the Development and Promotion of Science and Technology Talents Project (DPST, THAILAND) to pursue the master program at the School of Physics, Suranaree University of Technology under the supervision of Prof. Dr. Sukit Limpijumnong. He has published an article in an international journal and participated in several national and international conferences during the course of his master program education. Detail of the publication and abstracts of his presentations can be found in the APPENDIX.

